Universidade de Aveiro Departamento de Química
2018

BÁRBARA MAMEDE DE SOUSA

Estimulação *in vitro* de osteoblastos usando elétrodos interdigitados capacitivos para promover a osseointegração de implantes

In vitro stimulation of osteoblasts using capacitive interdigitated electrodes to improve implant osseointegration

Universidade de Aveiro Departamento de Química
2018

BÁRBARA MAMEDE DE SOUSA

Estimulação *in vitro* de osteoblastos usando elétrodos interdigitados capacitivos para promover a osseointegração de implantes

In vitro stimulation of osteoblasts using capacitive interdigitated electrodes to improve implant osseointegration

Dissertação apresentada à Universidade de Aveiro para cumprimento dos requisitos necessários à obtenção do grau de Mestre em Bioquímica – especialização em Métodos Biomoleculares, realizada sob a orientação científica da Professora Doutora Sandra Isabel Vieira, Professora Auxiliar Convidada do Departamento de Ciências Médicas da Universidade de Aveiro e co-orientação do Professor Doutor Marco Paulo Santos, Professor Auxiliar Convidado do Departamento de Engenharia Mecânica da Universidade de Aveiro e do Professor Doutor José Alberto Fonseca, Professor Associado do Departamento de Eletrónica, Telecomunicações e Informática.

Este trabalho contou com o apoio do Instituto de Biomedicina (iBiMED) (UID/BIM/04501/2013), da empresa Micro I/O, Lda, e da Unidade LiM um nó da PPBI (Portuguese Platform of BioImaging, POCI-01-0145-FEDER-022122).

Por todos os trilhos, todas as águas da Ria e todos os portos de abrigo durante cinco anos.

Pelo apaixonante percurso na cidade de Aveiro.

Por toda a “Magia, Luz e Cor” que Aveiro sempre foi.

Por tudo isto, dedico este trabalho e o culminar deste percurso à minha fonte de força e a primeira e eterna inspiração, a minha Avó Odete.

o júri / the jury

presidente / president

Professora Doutora Maria do Rosário Gonçalves dos Reis Marques Domingues
Professora Associada com Agregação do Departamento de Química da Universidade de Aveiro

vogais / examiners committee

Doutora Ana Catarina Fernandes Marques
Investigadora de Pós Doutoramento no Instituto I3Bs da Universidade do Minho
(Arguente Principal)

Professora Doutora Sandra Isabel Moreira Pinto Vieira
Professora Auxiliar Convidada do Departamento de Ciência Médicas da Universidade de Aveiro
(Orientador)

agradecimentos / acknowledgements

O meu primeiro agradecimento é inevitavelmente dirigido aos meus orientadores. À Doutora Sandra Vieira, um enorme obrigada pela motivação constante para o percurso na área científica, pelas palavras motivadoras e todos os momentos marcantes. Ao Doutor Marco Santos, um grande bem-haja pela confiança depositada ao encaminhar este projeto para as minhas mãos e pela constante procura por mais e melhores resultados. À empresa Micro I/O, Lda e ao Doutor José Alberto, um agradecimento especial por possibilitar o arranque deste trabalho.

Ao João e ao Pedro, agradeço pela incansável companhia nesta jornada, pelo apoio em todos os momentos e pelo sentimento de "casa" que sempre me transmitiram quando a verdadeira casa estava tão longe. À Diana e ao Carlos, agradeço pela amizade intemporal e pelo apoio nos momentos certos, ainda que a quilómetros de distância. Ao Tiago e à Mariana, agradeço pelo prazer de acompanhar a vossa jornada e pelos ensinamentos mais marcantes quando menos espero.

À Rita e à Joana, as minhas maravilhosas colegas de casa, um enorme obrigada por tornarem este pequeno T3 numa verdadeira casa de família. Aos meus seis rebentos nesta academia – a Mariana, a Carla F., a Marta, a Carla L., o Rui e o Tiago – o mais sincero obrigada pela confiança depositada para vos apadrinhar nesta jornada universitária e pelos incentivos de força desde o primeiro dia. À Tânia S. um agradecimento especial pela companhia nesta "jornada óssea" e pela amizade que cresceu de forma tão bonita. À Tânia G. um agradecimento único pela amizade e pela companhia sempre presente nos últimos meses. Aos meus companheiros de jornada laboratorial com quem tive oportunidade de trabalhar no iBiMED um obrigada não chega pela ajuda e por todo o apoio.

Aos meus avós e aos meus tios, um agradecimento pelo amor e pelo carinho que a distância não diminui.

O meu maior agradecimento é sem dúvida aos meus pais, Elsa e Pedro, por tudo o que tornaram possível nestes 23 anos, por todo o amor e pela preocupação constante que os quilómetros não conseguem esconder.

Por último e talvez o melhor e mais importante, ao meu irmão Bernardo, a minha âncora nos momentos difíceis, um enorme obrigada por tudo o que partilhamos. És e serás a melhor parte de mim, agora e sempre.

palavras-chave estimulação eletromagnética, estimulador capacitivo de padrão interdigitado, osteoblastos, efeitos osteocondutores, osseointegração

resumo

A crescente incidência global de doenças músculo-esqueléticas e de cirurgias de revisão prostética, torna crucial o desenvolvimento de novas próteses ativas que incluam estímulos controláveis e permitam a osseointegração, evitando falhas na sua fixação. Idealmente, próteses ativas incorporam sistemas de atuação biofísica que promovem osteocondução e osseointegração. Estes poderão aplicar estímulos eletromagnéticos nos tecidos circundantes, dado que o osso possui naturalmente correntes elétricas endógenas. Vários estudos evidenciam efeitos positivos de estímulos exógenos elétricos e/ou magnéticos em remodelação óssea. Contudo, ainda não foram validados sistemas de estimulação que possam ser incorporados em implantes ósseos instrumentados ativos. Um novo conceito de estimulador capacitivo em co-superfície foi desenvolvido pelo nosso grupo, testando-se várias arquiteturas de elétrodos com diferentes designs – incluindo o padrão interdigitado. Neste trabalho pretendemos avaliar os efeitos osteocondutores *in vitro* da arquitetura interdigitada, usando um estímulo elétrico de alta frequência. Para isso, a proliferação e diferenciação de células pré-osteoblásticas MC3T3 foram analisadas após estimulação elétrica de 0.7 $V.mm^{-1}$ e 60 kHz, 30 min/dia durante 28 dias, usando a arquitetura de padrão interdigitado de reduzida espessura (0.1 mm). Os resultados indicam que a estimulação testada aumenta a produção e deposição de colagénio, a atividade da fosfatase alcalina e os níveis de mineralização da matriz. Os resultados obtidos serão comparados com resultados anteriores, no âmbito de uma análise sistemática dos vários parâmetros do estímulo (design dos elétrodos, intensidade e frequência de campo elétrico). Este trabalho incita ao estudo futuro da eficácia *in vivo* de estímulos de alta frequência, entregues por este estimulador capacitivo interdigitado implementado numa prótese ativa, no que poderá ser um futuro sistema de atuação terapêutica personalizada.

keywords electromagnetic stimulation, capacitive interdigitated patterned stimulator, osteoblasts, osteoconductive effects, osseointegration

abstract Given the growing global incidence of musculoskeletal disorders and the rising frequency of several prosthetic revision surgeries, it becomes crucial to develop new active prostheses that comprise controllable stimuli and allow for osseointegration, avoiding failures in implant fixation. Ideally, active prostheses will incorporate biophysical actuation systems that promote osteoconduction and osseointegration. These could apply electromagnetic stimuli to surrounding tissues, since the bone presents natural endogenous electric currents. Considerable research already revealed positive effects of exogenous electric and/or magnetic stimuli on bone remodelling. However, stimulation systems for incorporation in instrumented active bone implants are not yet validated. A new concept of capacitive cosurface stimulator was developed by our group, with several electrode architectures designed and tested – including the interdigitated pattern. The present study intends to assess the osteoconductive effects of the interdigitated electrode architecture *in vitro,* using high frequency electric stimulation. For such purpose, the proliferation and differentiation of pre-osteoblastic MC3T3 cells were experimentally assessed after electric stimulation of 0.7 $V.mm^{-1}$ and 60 kHz, 30 min/day for 28 days, using the thin interdigitated pattern architecture (0.1 mm thickness). The results show the tested stimulation setup increases collagen production and deposition, alkaline phosphatase activity and matrix mineralization levels. The obtained data will be compared with previous results to perform a systematic evaluation that correlates several stimuli parameters (electrode design, electric field intensity and frequency). This work drives future studies on the *in vivo* efficacy of high frequency stimuli delivered by these novel thin capacitive stimulators inserted in instrumented active implants, in what could be a future personalized therapeutic actuation system.

Contents

Figures index

Tables index

Abbreviations

A	ampere
ALP	alkaline phosphatase
ARS	Alizarin red S
ATCC	American Type Culture Collection
BCA	bicinchoninic acid
BMP	bone morphogenetic protein
BRU	bone remodelling unit
BSA	bovine serum albumin
C75BL/6	inbred strain of laboratory mouse ‘C57 black 6’
CC	capacitive coupling
ClC	chloride/proton exchangers
DAPI	4',6-diamidino-2-phenylindole
DC	direct current
DIV	days *in vitro*
DMSO	dimethyl sulfoxide
ECL	enhanced chemiluminescence
ECM	extracellular matrix

EDTA	ethylenediaminetetraacetic acid
EF	electric field
EP2	prostaglandin E2 receptor 2
EP4	prostaglandin E2 receptor 4
EX	voltage excitation
FACIT	Fibril-Associated Collagens with Interrupted Triple-helices
FBS	foetal bovine serum
FDA	Food and Drug Administration
FI	fold increase
GPCR	G protein-coupled receptors
HF	high frequency
HF ST	high frequency stimulation
HRP	horseradish peroxidase
IC	inductive coupling
IgG	immunoglobulin G
I/O card	input/output card
kDa	kilodalton
kHz	kilohertz
LF	low frequency
LF ST	low frequency stimulation
LSCM	laser scanning confocal microscopy
MAP	mitogen-activated protein
MC3T3-E1	osteoblast precursor cell line (derived from mouse calvaria)

MEM α	minimum essential medium – alpha modification
MF	magnetic field
mRNA	messenger RNA (ribonucleic acid)
MSC	mesenchymal stem cells
MSK	musculoskeletal
NADH	nicotinamide adenine dinucleotide (reduced form)
NADPH	nicotinamide adenine dinucleotide phosphate (reduced form)
NCP	non-collagenous proteins
ND	not described
NHE	sodium/hydrogen exchangers
NS	no stimulus
OD	optical density
PGE2	prostaglandin E 2
PBS	phosphate-buffered saline
PBS-T	phosphate-buffered saline Tween
ROI	region of interest
RT	room temperature
rpm	revolutions per minute
SDS	sodium dodecyl sulfate
SDS-PAGE	sodium dodecyl sulfate polyacrylamide gel
SPARC	secreted protein acidic rich in cysteine (osteonectin)
TBS	tris-buffered saline
TBS-T	tris-buffered saline Tween

TGF- β1	transforming growth factor β1
V	volt
VGCC	voltage-gated Ca^{2+} channels
WB	Western blotting
WR	working reagent

1 Introduction

Bone is a calcified, living, connective tissue that makes up most of the skeleton[1] – a multitasked structure where every bone works together, functioning as a system. Bones ensure levering for muscle action, with long bones supporting the muscular system and allowing locomotion, while flat bones surround and protect the vital organs[2]. Bone tissue is also a source of blood-producing cells[1] and plays a key role in homeostasis by regulation of acid-base balance and calcium and phosphorus serum concentrations, being the main source of the referred ions[3]. Moreover, bone stands out as a source for growth factors and cytokines – for example, osteoblasts produce several important factors for differentiation and survival of hematopoietic stem cells[4]. Generally, four main functions can be attributed to this connective tissue – support, movement, protection, and metabolism.

1.1 Macroscopic features of the skeleton and bone tissue

Any therapeutic approach designed for bone structures must consider bone dynamics within the human organism. Bearing this in mind, the comprehensiveness of macroscopic anatomy and associated interrelationships is vital for the central therapeutic aim of the project. Several features can be highlighted in the macroscopic anatomy of the complete skeletal system, as the general appearance and structural organization of each bone. However, the microscopical environment must also be broadly understood, since any physiological benefits will rise from changes at the cellular level, either inside the bone cells or in the extracellular mineralized matrix.

The human skeleton comprises 206 bones that are divisible into four classes: long bones, short bones, flat bones, and irregular bones[5]. The long bones are found in the limbs

and consist of a cylindrical diaphysis with the medullary canal as a central cavity, and limited in the extremities by two epiphyses – a model of long bones is illustrated in Figure 1a. Between the epiphysis and the diaphysis, the metaphysis stands out and it contains the growth plate (or epiphyseal plate) – a hyaline cartilage plate at each end of a long bone from where new bone grows[6]. The short bones consist of cancellous bone tissue covered by a thin crust of compact substance and are usually located in a part of the skeleton intended for strength and compactness[5]. The flat bones occur where the main requirement is either extensive protection for internal organs or provision of broad surfaces for muscular attachment. In those situations, bones are expanded into broad, flat plates, composed of two thin layers of compact tissue that enclose cancellous tissue between them[5]. The irregular bone consists of cancellous bone enclosed within a thin layer of compact bone and are grouped under a different description due to their peculiar form[5].

Long bones serve as a model for understanding the structural organization of bone tissue during bone development, growth, and bone remodelling for structural maintenance throughout life. As illustrated in Figure 1, the inner structure of long bones allows the distinction between two types of bone – compact or cortical bone and trabecular or cancellous bone - according to two distinct arrangements of the structural units – the osteons. Cortical bone is dense and composes the outer shell of all bones, surrounding the inner trabecular bone that consists of spicules enclosing the marrow cavity[1]. Macroscopically, cortical bone looks dense and solid while trabecular bone appears with a honeycomb-like network (Figure 1b).

Because of these arrangements, bone is histologically classified as a vascularized and innervated connective tissue that is enclosed by two distinct fibrous connective tissue membranes – the periosteum and the endosteum (Figure 1c). The periosteum is the external cover throughout the whole extension of bone, except for joints area where an articular cartilage is found instead. Within the periosteum, there are also nerve endings, osteoclasts, osteoblasts and their precursors, and blood vessels that nourish the bone. This outer membrane has the unique capability to generate new bone, hence a bone stripped of its periosteum will not survive[1]. Bone also contains the endosteum – an inner cover in direct contact with the bone marrow where blood vessels, osteoblasts and their precursors, and

osteoclasts are also found. The endosteum lines the marrow cavity in addition to enveloping the surface of trabecular bone and lining the blood vessel canals in the bone[2].

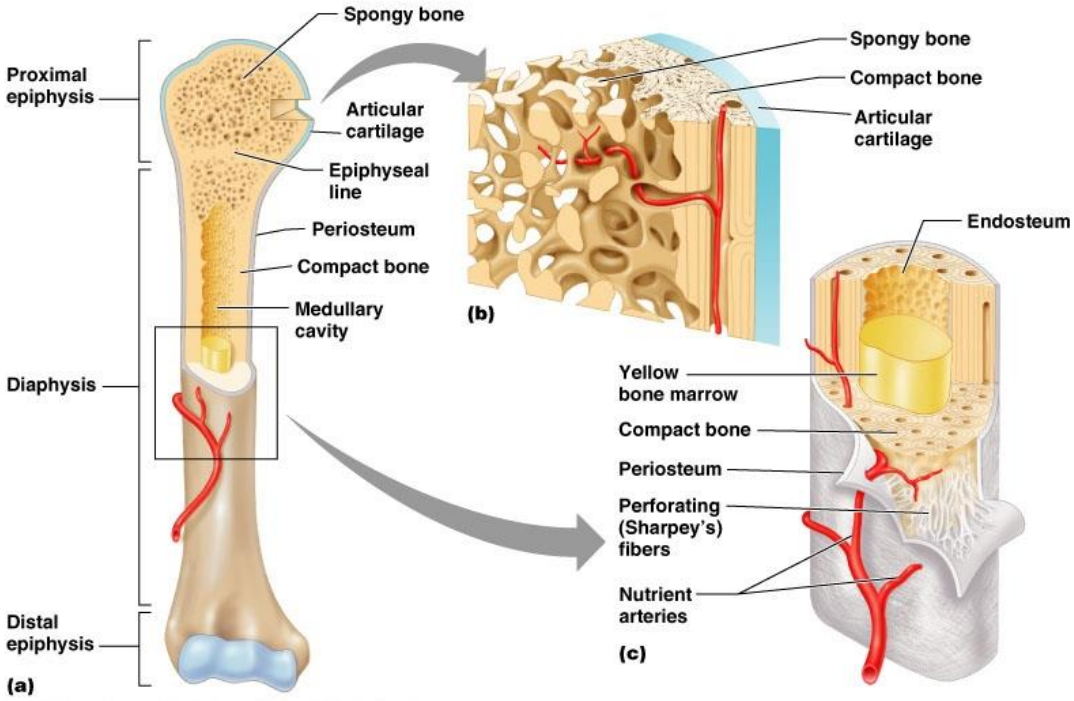

Figure 1 - a) Macroscopical Aspects of Bone. b) Compact vs Trabecular Bone. c) Periosteum vs Endosteum[7]

1.2 Bone development and maintenance

During bone development, all bones arise from mesenchyme[1] and two major modes of osteogenesis are distinguished, although both involve the transformation of a pre-existing mesenchymal tissue into bone tissue[2]. The direct conversion from mesenchymal tissue into bone tissue is named intramembranous ossification, a process that occurs mainly in skull bones[8,9]. The other process involves an intermediate stage in this conversion, where the mesenchymal cells differentiate primarily into cartilage, that is later replaced by bone – this process goes by the designation of endochondral ossification (Figure 2[8,9]). Bone appears in the 6-week-old embryo and its growth continues until circa 25 years old. Bone formation may still occur during adult life, although it requires remodelling[8]. Indeed,

the bones that form the skeleton of an adult human are sculpted by a modelling process and renewed by a complementary remodelling process[2].

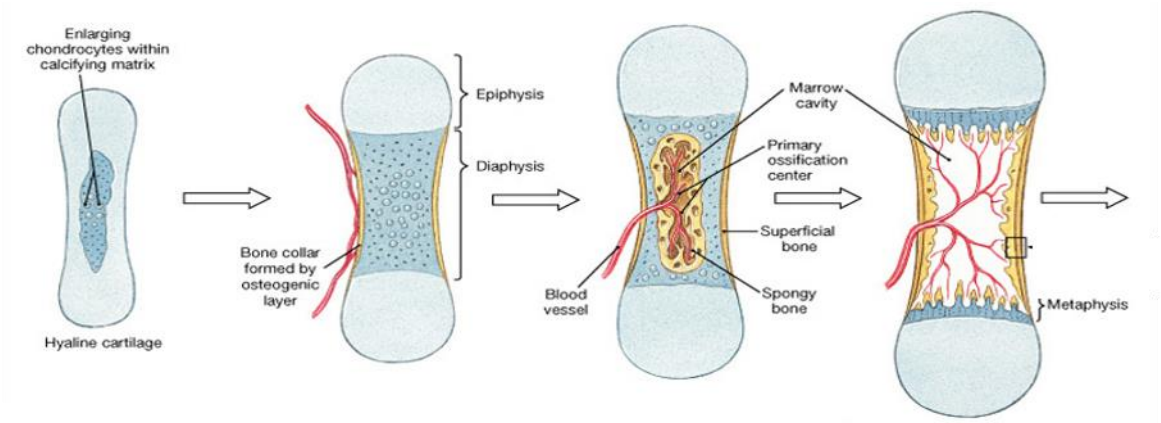

Figure 2 - Endochondral ossification step-by-step[8]

Bone modelling refers to a process through which bones are shaped or reshaped by combined but independent action of osteoblasts and osteoclasts. These modelling occurs mainly during growth in early ages or in adult life due to mechanical adaptation[2]. The bone's responsiveness to mechanical forces and regulatory signals are operative throughout life in order to maintain bone functions[10].

Bone tissue undergoes remodelling – a continuous process of resorption and renewal, which starts in the womb and continues until death. The remodelling process is essential for the maintenance of mineral homeostasis and preserves bone strength by replacing the old fatigued bone with a new mechanically sound one. This replacement is achieved by a sequential action of osteoclasts and osteoblasts with regulation by osteocytes[10]. In this process, bone formation is tightly coupled to prior bone resorption[2]. The rate of remodelling, as well as the balance between resorption and formation, differs depending on location, age, and disease state[10]. For a better comprehensiveness of the remodelling in bone tissue, the microscopic organization is further described.

1.2.1 Bone microscopic organization

Bone is a dynamic connective tissue containing an assembly of distinct cell populations required to aid its central role in mineral homeostasis, as well as its structural, biochemical and mechanical integrity. Bone comprises an intercellular calcified matrix, collagen fibres and a variety of cells within the matrix. The principal cells to stand out in the bone forming process are: the osteoprogenitor cells – responsible for maintaining the osteoblast population and bone mass; the osteoblasts – that synthesize the bone matrix on bone forming surfaces; the osteoclasts – that reabsorb bone and control the remodelling process; and the protective bone surface lining cells. The fidelity of bone tissue structure and metabolic functions depends on the exchange of regulatory signals among these cell populations[10].

i. Cells and signalling in initial bone formation

Bone formation involves osteoblast maturation, which in turn requires a spectrum of signalling proteins that influence selective gene expression throughout time, in order to direct osteoblasts' structural and functional properties during the differentiation process[10].

The bone marrow stroma contains multipotent mesenchymal stem cells (MSCs) (Figure 3) with proliferative potential, that under appropriate stimuli form osteoprogenitor colonies with the capacity to form bone[11,12]. Cells with similar features were also found in adult peripheral blood[13] and several foetal tissues[14]. MSCs are committed to tissue-specific cell types under the influence of signalling pathways and transcriptional regulators. The canonical Wnt/β-catenin pathway provides the initial cues to mediate gene expression aiming for skeletal development, bone formation and osteoblast differentiation[15,16]. Bone morphogenetic proteins (BMP-2, BMP-4 and BMP-7) are potent osteogenic inducers that also regulate gene expression[17]. The bone microenvironment provides a continuous supply of osteoprogenitor cells via accumulation of progenitor cell recruiters, such as circulating and osteoblast-synthesized cytokines, growth factors, non-collagenous proteins and other molecules, in its extracellular matrix (ECM). Further commitment and differentiation are induced by developmental proteins that signal transcription factors which activate

osteogenic genes, leading to the synthesis of a bone matrix that aids osteoblast's maturation[10].

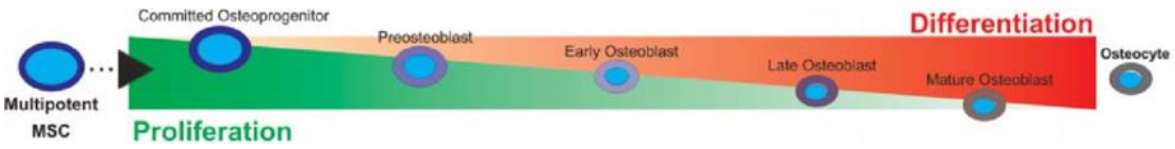

Figure 3 - Osteogenic differentiation from multipotent MSCs[12]

ii. Osteoblasts

Pre-osteoblasts are identified near the bone surface by histochemical detection of alkaline phosphatase enzyme activity (one of the earliest markers of the osteoblast phenotype). When a pre-osteoblast ceases to proliferate, key signalling events occur for its differentiation into an osteoblast. During osteoblast differentiation, three sequential stages can be distinguished throughout time as detailed in Figure 4: (1) proliferation, (2) bone matrix development and maturation, and (3) mineralization[18,19]. Studies covering the temporal expression of proteins provide a panel of osteoblast phenotypic markers that characterize each stage. The most frequently assayed markers include type I collagen, alkaline phosphatase, osteopontin, osteocalcin, bone sialoprotein and osteonectin. From the entire set, some proteins – like alkaline phosphatase – are early markers that increase as osteoblasts mature and deposit matrix, and decline with the transition to osteocytes. Inversely, other proteins, like osteocalcin, are late markers – associated with mineralization and being upregulated only in post-proliferative osteoblasts[10].

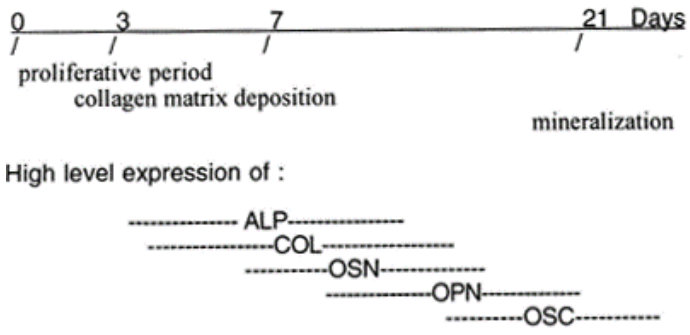

Figure 4 - Temporal expression pattern of osteogenic markers[19]

The active mature osteoblast is distinguished by its morphological properties, presenting a large nucleus, enlarged Golgi, and extensive endoplasmic reticulum – typical features of a cell engaged in the secretion of a connective tissue matrix. The osteoblast is also highly enriched in alkaline phosphatase and secretes type I collagen and specialized bone matrix proteins[18].

Bone lining cells are also observed and they either form the endosteum (separating bone from marrow) or underlie the periosteum directly on mineralized surfaces[10]. Both cell types (bone lining cells and osteoblasts) are in close contact by anchorage through the cytoskeleton – a combined effect of adherens junctions, tight junctions and desmosomes[20,21]. The cell-cell and also cell-matrix interactions are mediated by transmembrane and adhesion proteins[22] that are also involved in osteoblast differentiation[18]. The interrelationship between distinct cell types in bone tissue is illustrated in Figure 5.

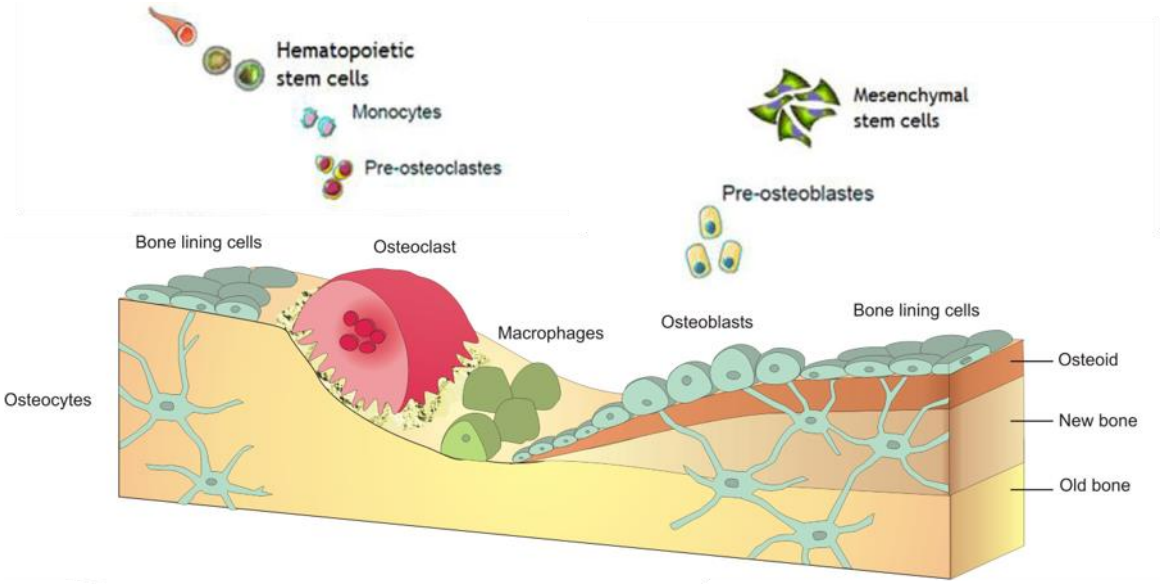

Figure 5 - Cell types in bone tissue[23]

The osteoblasts are responsible for the synthesis of the bone ECM, and the composition and organization of the bone ECM are essential for structural and functional fidelity of bone tissue. During the mineralization stage, the upregulation of non-collagenous proteins that act as calcium and phosphate binding proteins has a role in the ordered deposition of mineral, and regulation of hydroxyapatite amount[10].

iii. Extracellular matrix

Bone presents a connective tissue matrix that besides composing the largest part of the body's connective tissue mass, is unique by its constant regeneration throughout life as a result of bone turnover[24]. The bone matrix comprises several classes of proteins whose general features are already known.

The main matrix component is type I collagen, a triple-helical molecule containing two identical α1 chains and one α2 chain[25], with both chains characterized by several post-translational modifications and a well-known repeating triplet. Although bone matrix predominantly consists of type I collagen, collagen of types III and V as well as FACIT collagens (Fibril-Associated Collagens with Interrupted Triple-helices) may also be present in trace amounts during certain stages of bone formation, with a possible role on collagen fibril diameter regulation[24].

A small percentage (10 to 15%) of the matrix protein content corresponds to non-collagenous proteins (NCP). Some are serum-derived proteins – albumin and α2-HS-glycoprotein – NCPs with an exogenous origin that exert effects on matrix mineralization. Bone-forming cells synthesize and secrete NCP and collagen in equal amounts, and these NCP can be distinguished into proteoglycans, glycosylated proteins, cell-attachment proteins and γ-carboxylated proteins[24]. From this entire set of proteins, alkaline phosphatase (ALP) and osteonectin are glycosylated proteins that must be highlighted. ALP appears as one hallmark for bone formation and its deletion is known to cause an abnormal pattern of calcification[26]. Osteonectin is associated with osteoblast proliferation and matrix mineralization[27]. Concerning cell attachment mediators, bone cells synthesize at least nine proteins with this function. As main examples, osteopontin and bone sialoprotein perform roles in anchoring osteoclasts and osteoblasts to bone[26,28]. Bone matrix NCPs may experiment post-translational modifications by the action of γ-carboxylases, originating residues that enhance calcium binding[26]. One well-known example is osteocalcin, a valuable marker found in osteocytes that signals bone turnover cascade[29].

iv. Bone mineralization

Although with variable compositions when considering age, diet and health status, the mineral content generally accounts for 50-70% of adult mammalian bone, the organic matrix for 20-40%, water for 5-10% and lipids for <3%[24].

Bone mineral is an analogue of the geological mineral hydroxyapatite, and appears as extremely small mineral crystals that provide mechanical rigidity and load bearing strength to bone tissue. The crystalline structure of the mineral generates a reservoir for calcium, phosphate and magnesium ions[30]. The organic matrix, predominantly made up of type I collagen, guarantees elasticity and flexibility to the bone and determines its structural organization. Both collagen and its associated non-collagenous proteins influence the performance of both bone mineralization and bone remodelling. Water, found in the ECM and within the cells, is important for the maintenance of tissue properties and nutrition[24]. Moreover, cells that are responsible for bone formation, repair and remodelling usually respond to hormonal, mechanical and other extrinsic signals. Lipids are found as part of those cells' membranes and control the flux of ions, being directly involved in mineralization[24].

Initial mineral deposition is facilitated by ECM vesicles that help to accumulate calcium and phosphate ions and provide enzymes that degrade mineralization inhibitors, inducing apatite formation[26,31]. Osteoblast cells *in vitro* synthesize an ECM that mineralizes in the presence of an exogenous phosphate source. The synthesized matrix can be assessed by histochemical stains, namely von Kossa for phosphate and Alizarin Red for calcium. Bone matrix proteins may affect mineral deposition in cell culture and animal models, and their absence, modification or overexpression affects normal bone mineral properties. Considering such facts, it is apparent that bone cells, bone matrix and the extracellular environment can influence mineralization and the properties of bone related to mechanical strength[24]. The interrelationship between matrix, bone cells and the extracellular environment is depicted in Figure 6.

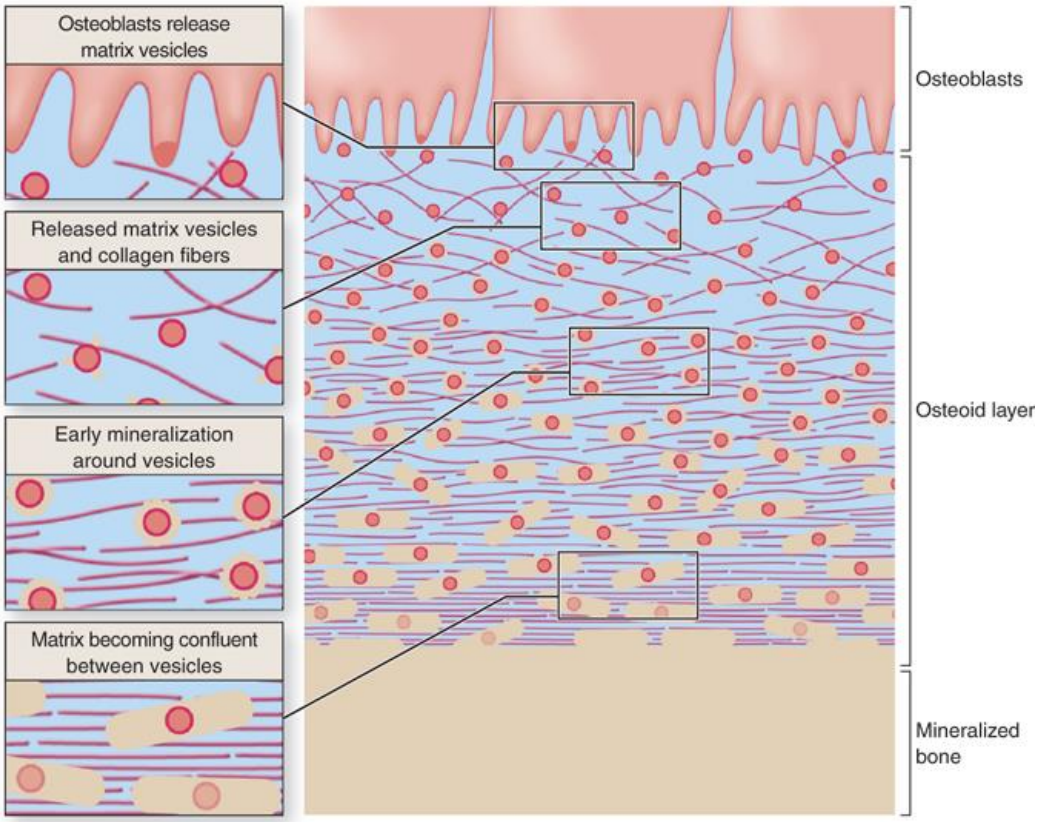

Figure 6 - Bone mineralization[32]

v. Osteocytes

The osteocyte is the final differentiation stage of the osteoblast and acts by supporting bone structure and metabolic functions. Osteocytes also represent the stage prior to cell death and morphological features, such as their filapodial processes, are quite distinguishing and allow for cytoplasmic connections with adjacent cells, either other osteocytes or surface osteoblasts[33]. Besides negative for alkaline phosphatase, osteocytes produce considerable amounts of osteocalcin and bone matrix proteins that may be involved in cellular extensions, as well as matrix molecules that support cellular adhesive properties[10].

Overall, the organization of osteocytes in direct contact with osteoblasts or surface lining cells shows that bone cells support bone structure, respond to physiological signals and can adapt those responses for bone formation and resorption[10].

1.2.2 Bone remodelling

Remodelling is achieved via a bone remodelling unit (BRU)[34,35] – a group of cells that undergo four distinct phases during the remodelling cycle (as illustrated in Figure 7): activation, resorption, reversal and formation.

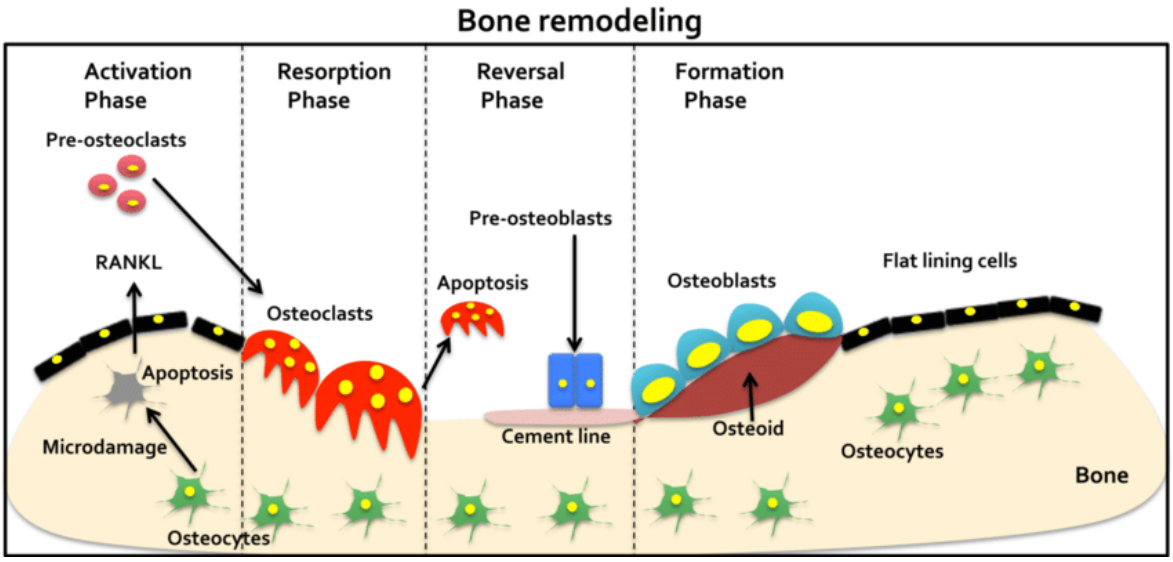

Figure 7 - Bone remodelling step-by-step[36]

(1) Activation is the initiating event to transform a quiescent bone surface into a remodelling one. Mononucleated osteoclast precursors are recruited from the circulation[37], infiltrate in the bone lining cell layer and fuse to form multinucleated pre-osteoclasts. There is some evidence that remodelling may be targeted toward particular sites, although most of it is likely to be random[38,39]. (2) In the Resorption phase, specific pumps of the osteoclasts transfer protons to the resorbing compartments lowering their pH. The acidification is accompanied by osteoclast secretion of lysosomal enzymes that are active at low pH and dissolve and digest the matrix, originating cavities on the surface of the cancellous bone as well as cylindrical tunnels within the cortex[2]. The resorption is performed by multi and mononucleated osteoclasts, ending with these cells' apoptosis[40]. (3) During the Reversal phase, monocytes and pre-osteoblasts are recruited to the resorption lacuna. All the coupling signals are released to summon osteoblasts and replace the bone that has been removed, so that an inefficient coupling mechanism would result in

bone loss. As the nature of coupling signals is undefined, one theory proposes that growth factors are released from the bone matrix by osteoclasts and perform as chemo-attractants for osteoblast precursors, stimulating their proliferation and differentiation[2]. Another hypothesis suggests that coupling is a strain-regulated phenomenon, and that remodelling occurs in relation to the mechanical loads and their resulting deformation (strain)[41]. As bone remodelling units cross cortical bone, a gradient of strain is created and osteoclasts are activated in response to reduced strain, while osteoblasts respond to increased strain[41]. (4) Formation is a two-step process through which osteoblasts synthesize the organic matrix and regulate mineralization. After secretion of the collagenous matrix, osteoblast release matrix vesicles that trigger mineralization establishing the optimal conditions for initial mineral deposition[2]. As bone continues to form, osteoblasts become buried in the matrix as osteocytes but still maintain contact between one another and with the cells on the bone surface. So, each osteocyte is part of a large three-dimensional and functional syncytium that "sense" changes in the mechanical properties of surrounding bone and regulates bone remodelling when necessary[42,43].

The net result after each remodelling cycle is the production of a new osteon and generally, the difference between the bone volume removed by osteoclast and that traded by osteoblasts is referred to as "bone balance"[44]. In cortical bone, the periosteal surface shows a slightly positive bone balance and with ageing, the periosteal circumference increases due to the cumulative effect of sequentially smaller positive balances. On the other hand, the endosteal surface shows a negative balance so that the marrow cavity enlarges with age. The net balance tends to be negative on the endosteal surface resulting in a cortical thickness decrease with age. As for the cancellous bone, the net balance is also negative causing a gradual thinning of the trabecular plates with age[2].

The primary function of bone remodelling is presumed to be the maintenance of mechanical strength through a continuous and preventive replacement of fatigued bone with new one[44]. Moreover, a second function is assigned to remodelling by providing access to calcium and phosphorus skeletal stores and hence having a crucial role in mineral homeostasis[2]. A final layout of the bone remodelling phases and the microenvironment of bone tissue with its distinct cell types is illustrated in Figure 8.

The normal turnover rate is around 2-3% per year in cortical bone – values that consist with the maintenance of mechanical properties. In cancellous bone, the turnover rate is much higher being this extra turnover destined to the role in mineral metabolism[2].

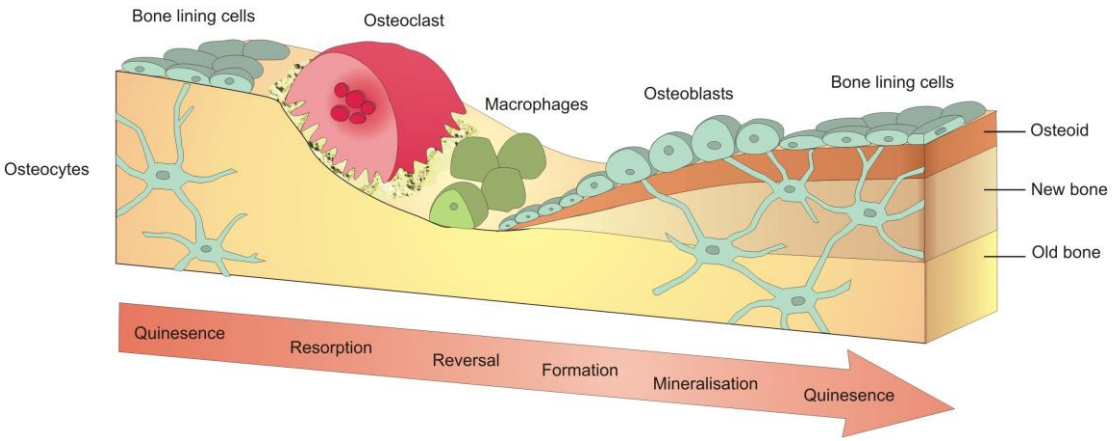

Figure 8 - Bone remodelling process and bone microenvironment[23]

1.3 Fracture healing and bone regeneration

Once a fracture occurs either by trauma or surgical intervention, the injured bone structure regenerates its original structural geometry and biomechanical integrity. Four phases comprise the fracture healing process as depicted in Figure 9: (1) inflammatory response; (2) mesenchymal stem cell recruitment and cell differentiation, leading to the formation of cartilage – the soft callus; (3) cartilage resorption and primary bone formation – the hard callus; and (4) secondary bone formation and remodelling in which the newly formed hard callus is shaped to restore the anatomical structure and support mechanical loads[45]. The molecular mechanisms that control the bone healing processes largely resemble those operating during the embryological skeletal development[46]. However, postnatal bone remodelling presents unique features that distinguish it from prenatal skeletal development. The inflammation and immune function play a substantial role in the initiation of bone healing. The disruption of the pre-existing skeletal unit defines a structural context where the bone regenerates with near-exact geometric and structural

attributes of the uninjured bone. Such regeneration occurs because morphogenetic factors act as defined by the pre-existing anatomy of the bone. Ultimately, the physiological and biomechanical conditions act as epigenetic modifiers of tissue morphogenesis and affecting the rate of fracture repair[45].

The fracture site sets up the spatial relationships during tissue regeneration, involving two circular shaped centres of cartilage formed on both sides of the fracture that taper proximally and distally along the bone cortices. Simultaneously, a crescent-shaped region of intramembranous bone formation is initiated in the periosteal tissues tapering inward towards the fracture. Hence, two distinct processes contribute to bone formation in fracture healing: one endochondral formation around the central region of the fracture and one intramembranous formation more peripheral and adjacent to bone cortices. The interactions in bone healing must occur among both referred formations, the external soft tissues adjacent to the fracture and the underlying cortical bone and marrow[45].

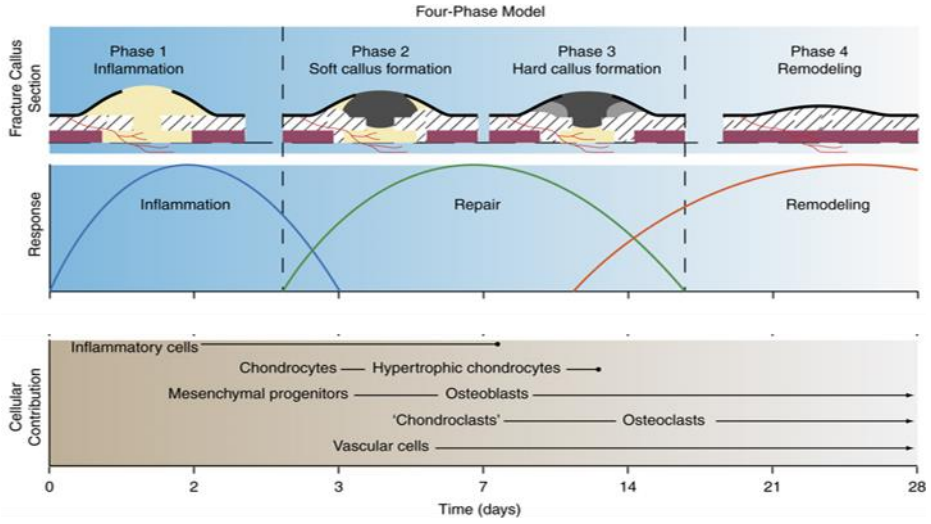

Figure 9 - Fracture healing process[45]

1.4 Skeletal disorders and Electric stimulation-based devices

The world's population is growing and people are generally living longer and are increasingly susceptible to chronic age-related diseases, including musculoskeletal (MSK) disorders[47]. MSK disorders were in 2010 the second most common cause of disability, accounting for more than 20% of the global burden[47–49]. This number has increased by 45% during the 20 years study period[48], both in developed and developing countries. The statistics and social impact of MSK disorders are expected to continue rising in the upcoming years and decades, mainly due to increasingly sedentary, obese and ageing population[50]. Successful methods to increase therapy effectiveness against these disorders are mandatory to pursue, as an urgent priority for health systems throughout the globe.

Surgical procedures are a common choice when MSK disorders are severe. The major challenge lies in the increasing number of surgical revisions when implant fixation and integration fails and leads to delayed healing or even to implant failures[51]. Osseointegration – a complex process that includes bone wound healing around the implant region[52,53] – is required for a long-term success of this implant-based therapy. Healing is promoted by the recreation of bone tissue microenvironment that contributes to maintaining homeostasis[54]. Biophysical stimulation is one essential component for the bone microenvironment, and this has encouraged studies on the application of biophysical cues – namely electromagnetic fields – to stimulate bone tissue regeneration and integration[54].

1.4.1 Electric stimulation in bone therapeutics

Studies on bone piezoelectricity first presented by Fukada and Yasuda have encouraged many other researchers to explore the effects of electric current on bone remodelling[55–57]. Prominently, several authors have reported the efficacy of electromagnetic stimulation to prevent and even reverse osteoporosis in animal models[58,59]. Osteoporosis, one of the major MSK disorders, is characterized by low bone mass and structural deterioration due to imbalanced bone remodelling[60].

Indeed, musculoskeletal tissues respond to biophysical stimuli, including to electromagnetic fields. Fukada and Yasuda first described that a mechanical loading stronger enough to cause deformity generates electric potentials[61]. Mechanical loading forces drive bone shape, and either attempt to elongate or shorten bone, as a function of tension or compression patterns, respectively[61,62]. In areas under compression the potentials are electronegative and cause bone resorption, while in tension areas the potentials are electropositive and cause bone formation[61,63]. Subsequent studies were designed considering that exogenous electric stimulation of these endogenous potentials would enhance bone healing[64]. In fact, exogenous electromagnetic stimuli applied to injured bone tissues mimic endogenous potentials and tend to improve and enhance the physiological healing response[65,66].

Besides mechanical loading effects, electromechanical properties are also influenced by the bone composition and macrostructure – as cortical or trabecular bone present differing electric and/or dielectric properties[67–69]. Such properties are intrinsic to the bone structure and expressed if externally excited[70]. Also, intrinsic factors such as tissue age and mineral and organic content influence interactions with electric currents and determine bone dielectric properties[71,72]. Electric currents and potentials provide important biophysical input to connective tissue cells, regarding mechanical competence and needs of the ECM[70]. However, an injured musculoskeletal tissue that starts to heal presents disorganized currents, and the healing response needs to be improved[65].

Bone electric and/or magnetic stimulation may also support osseointegration, one of the most important phenomena affecting long-term behaviour of uncemented orthopaedic implants[73]. A strong and durable mechanical bond between the prosthetic component and the host bone is highly desirable[74,75] and long-term success is influenced by the biological response of the host tissue to the implant presence[76]. Bone-implant interfaces cannot ensure a timeless stable performance when interfacing bones structures in which their quality is time-related (including osteoporotic states), so maintenance of adequate peri-prosthetic bones is a key factor[73,76]. Loss of primary stability and early migration of the implant occurs frequently, which can result in implant loosening and unavoidably revision procedures – the only possible therapeutic option in many cases[77–79].

Considering therapeutic applications, electric fields present several advantages over alternative approaches, such as the use of pharmaceutical drugs and (bio)chemical modification of the implant surface, including the absence of toxic chemicals and the absence of immune responses in host tissues. Applications of this kind are cost-effective and require uncomplex electromechanical technologies[80]. Electrodes can be further incorporated in implants and this incorporation allows for repeated treatment in the same target area and monitoring of such area, as well as the ability to deliver therapeutic actuation after the implant insertion, the ability to control therapeutic actuation in a personalized basis, among other advantages[80]. Moreover, electric fields involve little cell handling[81] – since electric field actuation does not require physical manipulation of the surrounding tissues when applied *in vivo*, neither requires cell handling throughout stimulation assays *in vitro*. Instrumented active implants, with the ability to apply personalized electrical and/or magnetic stimuli in the bone-implant interface, represent an innovative concept to control bone regrowth and optimize osseointegration[51,80]. Furthermore, their application can be quite significant when revision procedures endanger the patients' life or deeply deprive their life quality, especially for active and young patients and those suffering from osteoporosis[78] (notice the increasing number of young patients that currently represents 30% of the overall patients, but can exceed 60% in the next decade[82,83]).

1.4.2 Electric stimulation devices

As stated above, exogenously delivered electric stimulation will most likely mimic normal endogenous electric currents[66]. Devices based on such stimulation aid bone remodelling and fracture healing by guiding electric or electromagnetic currents[65] or defining suitable electric field distributions and strengths through bone-implant interfaces of implants not yet integrated[84].

The Food and Drug Administration (FDA) has approved stimulation of bone growth through active osseointegrative devices based on three methods for administration of biophysical electromagnetic stimuli. Devices can be designed to deliver electric currents by direct coupling (DC), electric fields by capacitive coupling (CC) and magnetic fields by inductive coupling (IC)[63]. The DC method is invasive while both CC an IC methods are

non-invasive (are not in direct contact with the stimulated cells or tissue). The effectiveness of these methods has been demonstrated both *in vivo* and *in vitro*, and they have been proposed as therapeutic strategies to minimize loss of bone mass, promoting bone fracture healing and improving osseointegration in bone-implant interfaces[59,85–87].

The remodelling potential of electrical and magnetic stimulation *in vitro* has already been proved using the three stimulation methodologies. However, only isolated trends for electrical stimulation treatment have been established[63,88]. To date, bone stimulation is an effective treatment, but further studies are required[89]. Future comparative studies between different types of stimulation that can promote osteoconductivity would optimize the clinical application – since uniform outcomes (rather than isolated trends) could be established[63,89]. IC stimulation has been the most described and used methodology[90]. Nevertheless, the tested IC magnetic stimulation architectures require very high electric current excitations (usually exceeding 1 A) to ensure the delivery of osteoconductive magnetic flux densities, which is a critical problem for self-powering, stand-alone and long-term operation of advanced instrumented implants[91,92]. The positive osteoconductive outcomes from the few *in vitro* studies using the less explored CC stimulation should also be considered, as well as the ability of CC architectures to be miniaturized, their flexible integration and very low electric power requirements for efficient excitation[80]. Hence, with this work we aimed to expand evidence and test the ability of specific CC setups to provide osteoconductive stimuli to osteoblast cells *in vitro*, aiming for their incorporation in advanced stimulatory architectures inserted in future sophisticated bone implants.

1.5 A new *in vitro* CC stimulation model

In vitro studies in bone cells are the first option to test osteogenic parameters for further use in DC, CC and IC devices and explore specific features in bone remodelling, by assessing osteoblastic maturation in culture. Osteoblasts are the main cells used, as these are responsible for bone matrix production[93]. Considering the approved stimulation methods, several literature data are available on experimental designs and biological outcomes for *in vitro* stimulation[63,65,66,89]. The final biological outcome after electrical stimulation is strongly influenced by both the stimulus characteristics – stimulation

method, as well as stimuli waveform, frequency, strengths of electric or magnetic fields (EF or MF), etc. – and the biological set up – as cell model, cell density and maturation stages[51,80].

CC stimulation has been proved as a suitable stimulation method for delivering electric fields (EFs) to cultured cells and to promote osteoblastic maturation *in vitro*. Studies from our research team included surveys on the characteristics of CC apparatus[94] and already described CC stimuli characteristics capable of inducing positive effects on bone cells *in vitro*. Most CC studies described osteogenic effects for frequencies lower than 100 Hz, mostly below 20 Hz, except for an outlier frequency value of 60 kHz that induced bone cells proliferation[51,95,96]. The EFs strengths presenting osteogenic effects ranged from $1x10^{-7}$ to 210 $V.cm^{-1}$ but most CC studies were performed using EF strengths between 13 to 60 $V.cm^{-1}$ (that generally increased proliferation)[97]. At the cellular level, weak EFs seem to be ideal over strong ones as they can induce beneficial responses without damaging the cells, while resembling the endogenously produced EFs in bone tissues. At the technological level, the weaker the EF the better, as higher electrical voltage excitations are required when delivering higher EF and high voltage generation is hard to achieve within self-powering implantable medical devices[51,98].

The increasing demand for stimulation systems that aid osseointegration around bone-implant interfaces has driven us to develop new CC stimulation systems based on cosurface design. The new concept of a cosurface-based capacitive system uses electrodes on the same surface to deliver the EF stimuli. The coplanarity itself is technologically advantageous for effective incorporation within intra-corporeal bone implants, and the system can comprise as many electrodes as required – each functioning independently. Furthermore, the electrodes can be shaped with arbitrary geometries and separated from adjacent electrodes by variable gaps. Implantable devices based on this cosurface concept can deliver controllable and personalized electric field stimuli to target tissues[51].

A prototype architecture of this system was constructed for *in vitro* tests by a research group from the Centre for Mechanical Technology and Automation (TEMA) at Universidade de Aveiro. A group of researchers from the Institute for Biomedicine (iBiMED) at Universidade de Aveiro tested the osteoconductive properties of this

prototype. Successful results were obtained for osteoblastic proliferation and differentiation using a cosurface stimulator with the striped pattern (depicted in Figure 10 and Figure 11)[51]. Both stimuli characteristics tested had positive (although some different) osteoconductive properties: low frequency stimulation (LF ST; 14 Hz for 4 hours/day) appears to induce collagen deposition into the matrix and to slightly increase matrix mineralization at 21 days *in vitro* (DIV); high frequency stimulation (HF ST; 60 kHz for 30 minutes/day) led to increased procollagen secretion in stimulated cells at 7 DIV but most significantly at 14 DIV, and decreased mineralization at 21 DIV. As a general trend for both stimulation frequencies, a major increase in type I collagen levels (1.8-2.7 times) was verified at 7 DIV but most prominently at 14 DIV timepoint (and specifically for HF ST as stated above)[51].

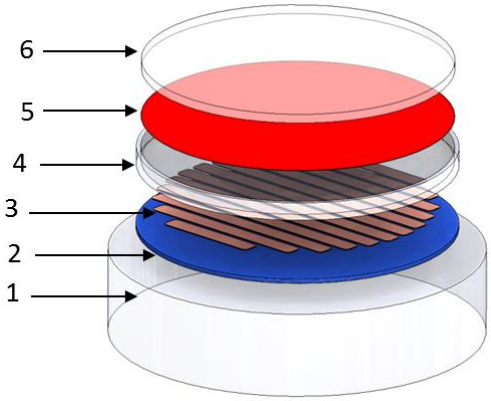

Figure 10 – Schematic representation of the cosurface stimulator with a striped pattern. 1 - Air; 2 - Polymeric substrate; 3 - Electrodes; 4 – Culture dish; 5 - Cellular layer (proliferation stage) or cellular tissue (differentiation stage); 6 – Culture medium (a liquid solution).

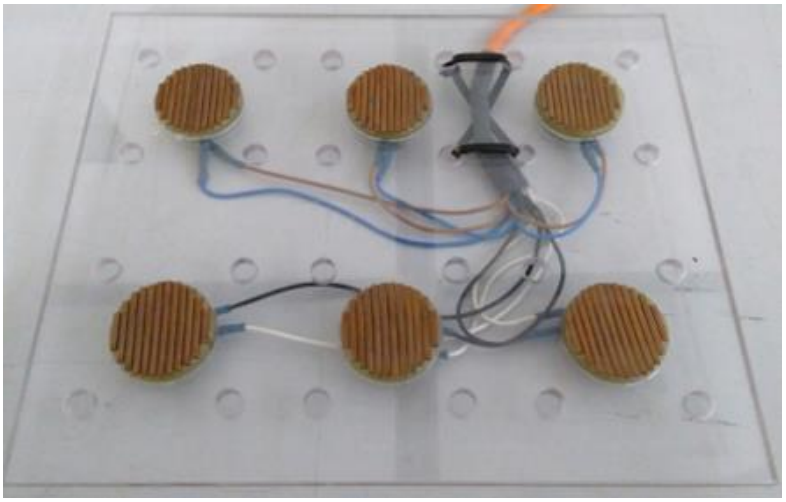

Figure 11 - Overall apparatus for in vitro experiments, comprising 6 individual striped stimulators

Maintaining the advantageous architecture of cosurface capacitive stimulation, another prototype was assembled using an interdigitated pattern with 0.1 mm of thickness. The ability to deliver controllable stimuli was numerically computed by computational analysis prior to any *in vitro* tests. Novel advantages stand out in this newly assembled pattern, since electrode thickness is now ten times lower than the initial 1 mm thickness of the striped-type electrodes. To achieve a trustworthy comparison, the same low and high frequency stimulations had to be tested for the interdigitated pattern. The *in vitro* osteoconductive properties of an electrode with an interdigitated pattern were already tested in our lab (unpublished data). This study compared the osteoblast proliferation, maturation and mineralization efficiencies in unstimulated cells versus LF ST (low frequency stimulus) stimulated cells. The work performed in this dissertation intended to complete our data on the osteoconductive properties of CC interdigitated electrodes, by performing experimental studies now testing HF ST (high frequency stimulus).

2 Aims

The present dissertation lies on a major purpose: to analyse the stimulatory ability of *in vitro* interdigitated capacitive stimulation apparatus for future assembly on innovative bone instrumented implants. To achieve this purpose, the stimulation system was optimized towards effective osteoconductive effects so that innovative therapeutic solutions will hopefully control osseointegration, preventing or treating aseptic loosening, to ultimately avoid the need for surgical revisions. Hence, the following specific objectives were established:

(i) to evaluate the effects of high frequency stimulation by thin interdigitated electrodes on MC3T3 pre-osteoblast cells' proliferation.

(ii) to evaluate the effects of high frequency stimulation by thin interdigitated electrodes on the matrix maturation of MC3T3 pre-osteoblasts.

(iii) to evaluate the effects of high frequency stimulation by thin interdigitated electrodes on the matrix mineralization of MC3T3 pre-osteoblasts.

(iv) to compare the complete set of results here obtained for high frequencies with our unpublished results for low frequencies using the interdigitated stimulator pattern and our published data using the striped stimulator pattern.

3 Materials and Methods

3.1 Capacitive stimulation apparatus and electric stimulus specifications

As defined in section 1.5, the interdigitated stimulator used in this work maintains the cosurface design, with both electrodes (one positively charged and the other grounded) being in the same geometric plane. The capacitive stimulator is designed to stimulate a region of interest (ROI) defined as the cell culture and its medium, in a 35 mm diameter cell culture plate. In this cosurface configuration, the dielectric is not limited to the gap between electrodes but extends to the overall volume that can be polarized by the EFs. Electrodes were fabricated in copper due to its very high electrical conductivity.

The interdigitated capacitive-coupled stimulator responsible for EF delivery to cell models in culture has been previously designed and is here characterized. The complete configuration comprises two electrodes, each one presenting ten strips. The complete set of ten strips from one electrode fits the intermediate blank spaces between the ten strips of the complementary electrode. Each electrode is 0.1 mm thick and 1 mm wide for each strip, except for the extremity ones that present a 2 mm width. This pattern was designed as a set of tracks of a printed circuit board, which was achieved by etching the conductive pattern on a copper clad laminated FR-4 substrate (PCB fabrication). As illustrated in Figure 12, strip length is variable with a constant inter-electrode space of 0.5 mm, such that the EF stimuli can be delivered to the entire cell culture. Each interdigitated stimulator was positioned over the FR-4 substrate and the cell culture dishes placed on top of them – ensuring no direct contact between cells and electrode. The overall apparatus for *in vitro* testing includes 6 individual interdigitated stimulators available for stimulation at the same time, as shown in Figure 13.

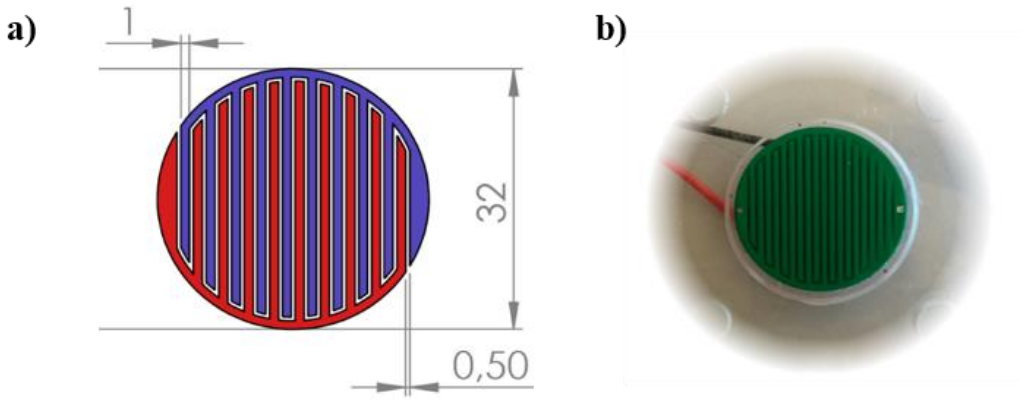

Figure 12 - Interdigitated electrode configuration and dimensions. Schematics on the left image and final assembly in the incubator on the right image. Electrodes in red colour were positively charged; electrodes in blue colour were grounded.

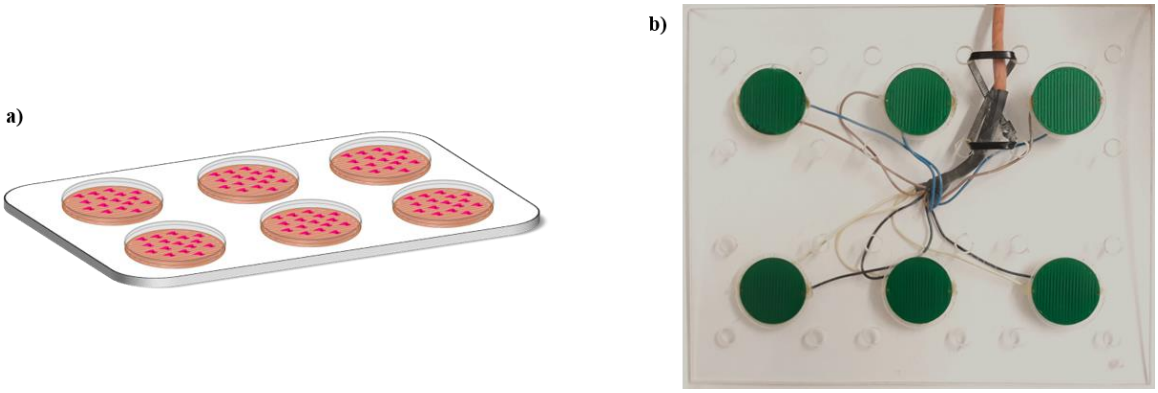

Figure 13 - Overall apparatus comprising 6 individual interdigitated stimulators – a) schematics with cell culture dishes above each electrode and b) final assembly.

Upon supply of an electric potential difference (voltage) – defined by supply parameters such as amplitude, frequency, periodicity, supply duration and activation and resting time – an EF was delivered to the cells – defined by stimulation parameters such as strength, periodicity, duty cycle exposure, resting time and stimuli duration. A voltage excitation (*EX*) defined by 5 V amplitude (K_{EX}) and 60 kHz frequency (f_{EX}) was applied to drive the positively charged electrode, according to Equation 1 and Figure 14:

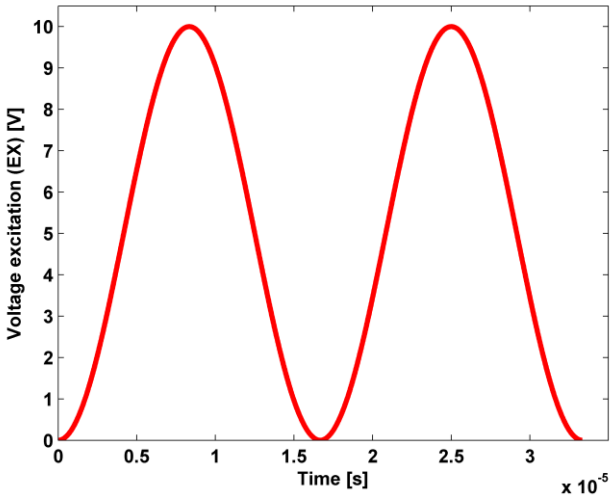

Figure 14 - Voltage excitation waveform (2 periods)

$$EX = K_{EX}\,(1 - \cos(2\pi f_{EX} t)) \qquad (1)$$

These parameters were similarly defined as in the previous study conducted by Soares dos Santos *et al.*[51] for cell stimulation using striped planar electrodes. A previous study conducted in our lab analysed the bioactivity effects of low frequency stimulation using the interdigitated pattern. Hence, for comparative purposes, the voltage amplitude was kept at 5 V.

Excitations to power electrical stimulators were configured using a real-time application, which was developed using Simulink (v. 7.3, Mathworks) and the Real Time Workshop (v. 7.3, Mathworks) and run using the Real Time Windows Target (v. 3.3, Mathworks) kernel. Excitations were generated by an I/O card (MF 624, Humusoft)[51].

A finite element computational model was implemented using COMSOL Multiphysics (v. 5.3, COMSOL) to predict the electric field stimuli delivered to bone cells when electrodes were driven by the *EX* excitation. This model was developed considering an *in vitro* stimulation apparatus as illustrated in Figure 15, which has been used to analyse electromagnetic stimuli delivered *in vitro* to several cell lines[51,91]. It comprises 6 domains: culture medium (1 mm thick), cellular layer (proliferation stage; 10 µm thick) or cellular

tissue (differentiation stage; 20 µm thick), culture dish (0.5 mm thick), electrodes (0.1 mm thick), FR-4 substrate (0.5 mm thick) and air (9.5 mm height). The differentiation stage was modelled using a double thickness of the adherent organic layer in comparison with the proliferation stage, in order to approximately consider the organized cellular tissue mainly composed of MC3T3 cells and type I collagen. The interdigitated pattern used for EF stimulation[51] was designed considering the electromagnetic properties of organic and inorganic materials composing the system defined in Figure 15.

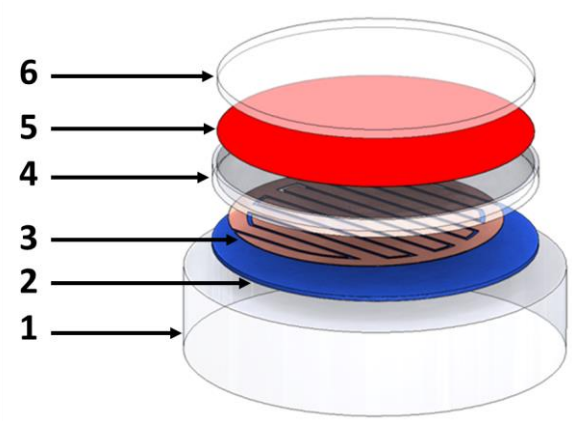

Figure 15 - Schematic representation of the cosurface stimulator with an interdigitated pattern. 1 - Air; 2 – FR-4 substrate; 3 - Electrodes; 4 – Culture dish; 5 - Cellular layer (proliferation stage) or cellular tissue (differentiation stage); 6 – Culture medium (a liquid solution).

Frequency- and region-dependent EF stimuli are delivered to bone cells, as shown in Figure 16 and Figure 17. Stimuli distribution and strength along the cellular layer and along the cellular tissue are quite similar. As presented in Figure 16, HF stimulation delivers approximately 2.3-fold higher EFs than LF stimulation (maximum stimuli: 0.3 $V.mm^{-1}$ vs 0.7 $V.mm^{-1}$). These maximum EFs are imposed on the cellular layer/tissue above the positively charged electrodes; minimum EFs occur over the grounded electrodes.

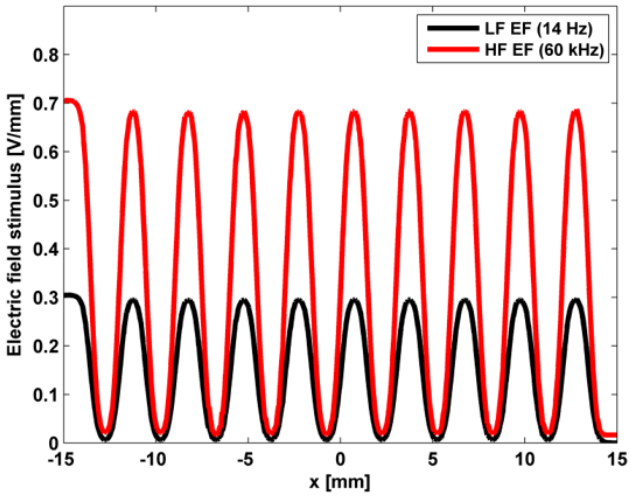

Figure 16 - EF stimuli distribution and strength along the cellular layer (proliferation stage) and along the cellular tissue (matrix maturation stage) in the x-plan (y=0, i.e., throughout a perpendicular line to the electrodes orientation)

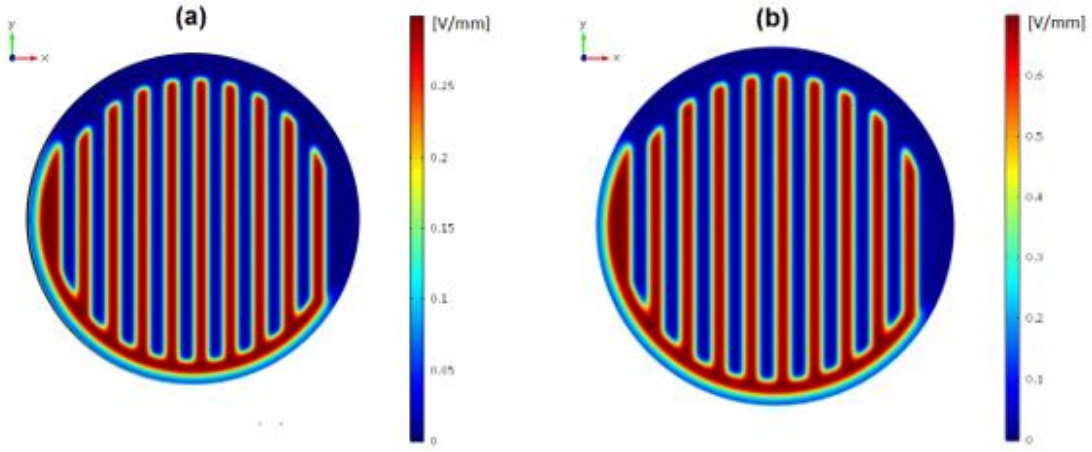

Figure 17 - EF stimuli distribution and strength along the cellular layer (proliferation stage) and along the cellular tissue (matrix maturation stage) in the xy-plan (horizontal plan in the cellular layer/tissue midpoint): (a) LF stimulation; (b) HF stimulation

The experimental apparatus for EF stimulation is illustrated in Figure 18. On the left side of the image is depicted the control station (that includes the I/O card), which controls the delivery of stimuli in real time; and the signal generator, that ensures the generation of the high frequency excitations. On the right side of the image is represented the New Brunswick Scientific CO_2 instrumented incubator where the stimulator sets are

placed. Cell culture dishes that receive electrical stimulation are placed above each stimulator on the top shelves and the control cultures are placed in the ground shelf.

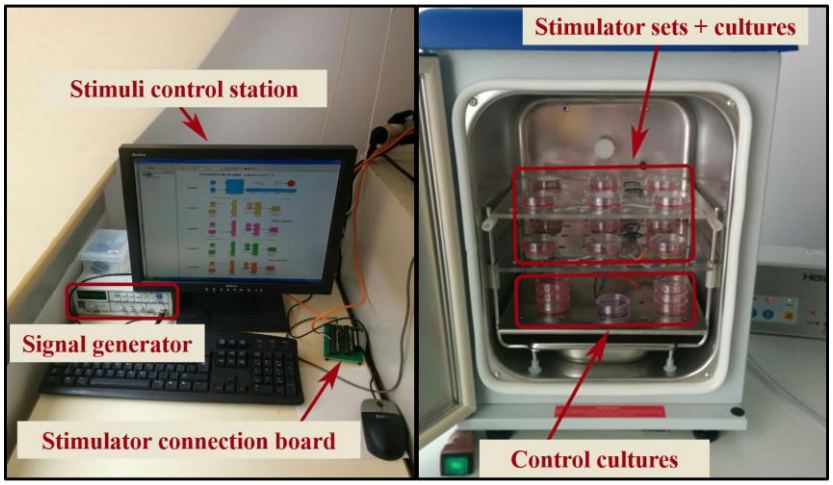

Figure 18 - The experimental apparatus for EF stimulation. On the left, the control station (including the I/O card) and the signal generator. On the right, the incubator equipped with the stimulator sets.

3.2 Biological outcomes assessed

Various biological outcomes can be assessed to evaluate the effects of electric stimulation on the proliferation and differentiation yields of bone cells in culture. The assessment of these biological outcomes can be categorized according to the three specific stages of *in vitro* osteoblast differentiation: (1) proliferation, (2) maturation, and (3) matrix mineralization[99,100]. (1) Proliferation is assessed by cell counting, cell viability assays and protein synthesis quantification. (2) Maturation involves osteoblast differentiation and formation of an organic matrix, being evaluated by the expression and localization of matrix-associated proteins. Type I collagen is the gold-standard choice for assessment[101,102], but non-collagenous proteins such as osteonectin, osteopontin, osteocalcin and bone sialoprotein can be used as well. Osteonectin and osteopontin mediate signal cascades required for full expression of the mature osteoblast phenotype and ECM mineralization. The expression and activity of ALP are also biomarkers for osteoblasts differentiation; this enzyme increases phosphate concentration to the required level for hydroxyapatite crystal generation and, besides being an osteoblast early marker,

ALP levels and activity increase until osteoblastic maturation is complete[103,104]. (3) Mineralization can be inferred by measurements of osteocalcin expression, and of the amount of extracellularly deposited calcium (via e.g. Alizarin red assay) or phosphate (via e.g. the Von Kossa assay). Osteocalcin is a non-collagenous protein secreted by osteoblasts that combines with hydroxyapatite in the presence of calcium, to modulate crystal morphology[104–106].

Each assay lasted 28 days and during the complete assay, cell cultures were subjected to high frequency (60 kHz) stimulation for 30 minutes each day. Throughout the experimental period, the biological outcomes were monitored at defined timepoints (days *in vitro*, DIV) according to Table 1. The experimental details of the biological assays are presented in the subsequent sections.

Table 1 – Summary of performed assays, timepoints per assay and biological processes assessed.

Assay	**Days *in vitro* (DIV)**	**Biological outcome / Biological stage**
Resazurin assay	1, 3, 5, 7, 14, 21, 28 DIV	Cellular viability and metabolic activity / Proliferation
ALP activity assay (secreted)	7, 14, 21, 28 DIV	Activity of secreted ALP / Maturation
WB assays of conditioned media (secreted protein markers)	1, 3, 5, 7, 14, 21, 28 DIV	Expression and quantification of relevant secreted osteogenic protein markers / Maturation and Matrix mineralization
WB assays of cell lysates (cellular protein markers)	7, 14, 21, 28 DIV	Expression and quantification of relevant cellular osteogenic protein markers / Maturation and Matrix mineralization
Immunocytochemistry (cellular and ECM protein markers)	21, 28 DIV	Expression and localization of relevant osteogenic protein markers in cells and mineralized matrix / Matrix mineralization
Alizarin Red assay	21, 28 DIV	Visualization of calcium deposits / Matrix mineralization

3.2.1 Culture and maintenance of the MC3T3-E1 cell line

The osteoblastic MC3T3-E1 cell line, a non-transformed cell line established from the C57BL/6 newborn mouse calvaria, displays osteoblast-like characteristics and is one of the most used cell lines in *in vitro* electromagnetic stimulation experiments. These cells are considered a suitable model to study the sequential transition from proliferation to differentiation, and molecular mechanisms underlying both the osteoblastic maturation and the formation of bone-like extracellular matrix[107].

The MC3T3-E1 subclone 4 (CRL-2593, ATCC, Barcelona, Spain) was used in this study. It has a similar behaviour to primary calvarial osteoblasts, with high level of osteoblast differentiation and ability to form a well mineralized ECM. MC3T3-E1 cells were maintained in an incubator at 37 ºC and a humidified atmosphere of 5% CO_2, using the recommended culture medium: 2 mM L-glutamine-containing Minimum Essential Medium alpha (MEM α) in Eagle's balanced salt solution, supplemented with 2.2 $g.L^{-1}$ sodium bicarbonate ($NaHCO_3$), 10% (v/v) Foetal Bovine Serum (FBS) – heat inactivated, South American origin – and 1% (v/v) of an antibiotic-antimycotic solution (10,000 $units.mL^{-1}$ penicillin; 10,000 $\mu g.mL^{-1}$ streptomycin and 25 $\mu g.mL^{-1}$ Amphotericin B) (Gibco BRL, Invitrogen, Life Technologies, USA).

Cellular subculture was performed using 0.05% trypsin/EDTA (Gibco BRL, Invitrogen, Life Technologies, USA), with cells being split at 70-80% confluence (sub-confluent state). After seeding on test culture dishes, medium renewal was performed every 3 days for every dish under stimulation or control settings. *In vitro* electric stimulation was carried out in a CO_2 instrumented incubator (Galaxy 14S, New Brunswick Scientific, Eppendorf Group, Germany) equipped with the capacitive stimulation apparatus and a communication port to deliver electric signals to electrodes. Enhanced proliferation is expected to occur when cells are stimulated in the 'log growth' phase, i.e., when the stimulus is applied in non-confluent cultures[97,108].

3.2.2 Trypan Blue assay for initial cell seeding

MC3T3-E1 cells were seeded on 35 mm cell culture dishes according to a defined density – $1x10^4$ cells.cm^{-2} – corresponding to ~10 % confluence. A dye exclusion assay that distinguishes the viable cells from the dead ones, allows plating of a defined number of living cells in each cell culture dish. Living cells exclude the dye as they present an intact cytoplasmic membrane, while dead cells stain blue due to reagent incorporation through the damaged cytoplasmic membrane. At the time of sub-culture, 10 µL of 0.4% Trypan Blue (Sigma-Aldrich, Dorset, UK) was added to a 100 µL aliquot of cell suspension and incubated for 1 minute at room temperature (RT). A haemocytometer (Neubauer improved) was used to count the viable (unstained) cells under an inverted microscope. The number of cells in the initial suspension was calculated for further cell plating, considering that a volume of 0.1 µL is housed by each 4x4 square of the Neubauer chamber.

3.2.3 Resazurin-based metabolic assay

A metabolic assay was performed at specific timepoints (referred in Table 1) to determine the proliferation of the cell population throughout the experimental period of 28 days. Resazurin salt (Sigma-Aldrich, Dorset, UK) is a cell permeable redox indicator, dissolved in phosphate-buffered saline (PBS) (Thermo Fisher Scientific, Pierce Biotechnology, USA) at a 0.1 mg.mL^{-1} stock solution. Cells were incubated during 4 hours with fresh complete medium containing 10% of this resazurin stock solution.

The viable and metabolically active cells keep a reducing environment within the cytoplasm and mitochondria due to mitochondrial enzymes such as NADPH dehydrogenase and NADH oxidoreductase, which are responsible for transferring electrons from NADH and NADPH to e.g. resazurin, which is reduced to resorufin. As the reduction reaction takes place, a change of colour from deep blue to pink occurs in the medium, and the amount of the final product (resorufin) can be monitored by absorbance and is proportional to the number of living cells in the sample[109,110].

After the incubation period, resazurin reduction was spectrophotometrically measured at 570 and 600 nm (Infinite 200 PRO, Tecan, Switzerland). The ratio between

the optical density (OD) at 570 and 600 nm is used to infer the cellular viability according to the following formula:

$$Viable\ cells\ (\%) = \frac{OD(570nm/600nm)_{[test\ cells]} - OD(570nm/600nm)_{[negative\ control]}}{OD(570nm/600nm)_{[positive\ control]} - OD(570nm/600nm)_{[negative\ control]}} \times 100 \quad (2)$$

In Equation 2, 'test cells' refers to the medium of cell culture dishes receiving stimulation); 'positive control' refers to the medium of cell culture dishes without electrical stimulation – illustrating the viability of the cell line under normal conditions; 'negative control' refers to culture medium with resazurin but without cells to reduce resazurin. The viability assay was performed at the referred timepoints, in 3-6 biological replicas.

3.2.4 Alkaline phosphatase activity assay

Alkaline phosphatase (ALP) is an enzyme that, when in an alkaline buffer, hydrolyses organic phosphates, increasing phosphate concentration. It is considered one of the most representative markers for osteoblast activity and differentiation. The enzyme plays a well-known role in hard tissue formation with high expression levels in mineralizing tissue cells.

The activity of secreted ALP was evaluated in the cell media at 7, 14, 21 and 28 DIV using ρ-nitrophenyl phosphate (Calbiochem, Merck, Germany) as a substrate for the enzyme. The substrate was diluted in an alkaline buffer solution (prepared as detailed in the Appendix section - ALP substrate solution). After incubating cell media with the ALP substrate solution for 1 hour in the dark at 37 ºC, the optical density of the enzymatic products was spectrophotometrically measured at 405 nm (Infinite 200 PRO, Tecan).

Since the amount of secreted ALP is low when compared with the amount of cellular ALP, this was also assessed by first using a PBS solution with 1% Triton X-100 (Calbiochem, Merck, Germany) for cell permeabilization. The cells in Triton solution were collected to a microtube, incubated for 30 minutes in an orbital shaker at 4 ºC and 200 rpm, followed by cell sonication for 30 seconds on ice, prior to the incubation with the ALP substrate solution.

3.2.5 Cell samples' collection and protein content quantification

Upon the indicated timepoints (Table 1), the cells' conditioned medium was collected to quantify and identify protein markers secreted by osteoblast-like cells throughout the complete length of the assay. At each timepoint, 500 µL of conditioned medium were collected from every culture dish (6 biological replicas) and 55 µL of 10% SDS (NZY Tech, Portugal) added to each sample, boiled for 10 minutes, and submitted to sodium dodecyl sulfate polyacrylamide gel (SDS-PAGE) and Western Blot (WB). The preparation of solutions used for SDS-PAGE and WB are detailed in the Appendix section (SDS-PAGE and WB solutions). Cells were lysed and harvested from culture dishes at 7, 14, 21 and 28 DIV to analyse the expression of some intracellular protein markers throughout the assay. 350 µL of 1% SDS were used at the 7 DIV timepoint, and 500 µL of 1% SDS in the other timepoints, in order to obtain similar lysate concentrations. For each timepoint, 5 biological replicas were collected and sonicated for 30 seconds prior to a boiling period for 10 minutes at 95 ºC.

The total protein content was quantified by the Pierce^{TM} BCA Protein Assay Kit (Pierce Biotechnology, USA) using an aliquot of each cell lysate, according to the manufacturer's instructions. The kit comprises a detergent-compatible formulation based on bicinchoninic acid (BCA) that allows for colourimetric detection and quantification of total proteins. The working method combines two reactions: (1) the reduction of Cu^{2+} to Cu^{1+} by proteins in an alkaline environment (the biuret reaction), with (2) the selective colourimetric detection of the cuprous cation (Cu^{1+}) by the BCA-containing reagent. The two combined reactions generate a purple product – a water-soluble complex with strong absorbance at 562 nm that arises from the chelation of two BCA molecules with one cuprous ion. The absorbance values of the BCA/copper complex are nearly linear with increasing protein concentrations over a broad range (20-2000 µg.mL^{-1}).

Generally, protein concentrations are determined with reference to standard concentrations of a common protein – bovine serum albumin (BSA). BSA standards were prepared (refer to Table 2) through a series of dilutions from a provided 2 mg.mL^{-1} stock solution. A standard curve was obtained by plotting BSA absorbance versus BSA

concentration; total protein concentration of each sample was inferred through the standard curve equation.

Table 2- Bovine serum albumin (BSA) standards used in BCA assay for total protein quantification - prepared from the stock BSA solution (2 mg.mL^{-1}). WR – working reaction.

BSA Standard	BSA stock (µL)	10% SDS (µL)	H_2O (µL)	Corresponding Protein mass (µg)	WR (uL)
P_0	-	2.5	22.5	0	200
P_1	1	2.5	21.5	2	200
P_2	2	2.5	20.5	4	200
P_3	5	2.5	17.5	10	200
P_4	10	2.5	12.5	20	200
P_5	20	2.5	2.5	40	200

Both cell lysates and standards were prepared directly into a 96-well microplate. In each well, biological samples were prepared in triplicate by adding 5 µL of each lysate to 20 µL of the solution used for sample collection (1% SDS). To each sample or standard well, 200 µL of the working reagent (WR) were added – WR is the mixture of BCA reagent A with BCA reagent B in a proportion of 50:1. The microplate is incubated in the dark at 37 ºC for 30 minutes and cooled at RT before gentle oscillation and absorbance measurement at 562 nm in a microplate reader (Infinite 200 PRO, Tecan).

3.2.6 Electrophoresis and Western Blot Assays

Cell lysates (mass-normalized by the BCA assay) and conditioned medium (viable cell-normalized by the resazurin data) samples were subjected to electrophoresis on a 5-20% gradient SDS-PAGE [29:1 Acrylamide:Bis-Acrylamid solution (Fisher Scientific, Ottawa, Canada)] and subsequently transferred onto nitrocellulose membranes for WB. For conditioned media samples, only the 5-20% resolving gel was electrotransferred; for cell lysate samples the 3.5% stacking gel was also transferred as it retains collagen fibres. A dual colour protein standard (Bio-Rad), was run in parallel with the samples to monitor

protein electrophoresis, confirm transfer quality and estimate the molecular weight of loaded samples.

After the electrotransfer, Ponceau S was used to stain protein bands to assess equal gel loading as well as quality control of proteins transfer to membrane[111]. The Ponceau S negative stain binds reversibly to the positively charged amino groups of the protein and to non-polar regions in the protein. Immediately after transfer, the nitrocellulose membranes were hydrated with 1x TBS for 10 minutes, followed by the incubation with Ponceau S solution (Sigma Aldrich, 0.1% [w/v] in 5% acetic acid) for 5 minutes, and a brief rinse in distilled water to make the bands visible in the membrane white background. The stained membranes were scanned in a ChemiDoc Imaging System (Bio-Rad) for further density analysis by ImageLab Software (Bio-Rad). Subsequently, membranes were washed with 1x TBS-T for 5 to 10 minutes until the red staining was totally eliminated. Membranes were immunologically detected afterward. The washing solutions used for nitrocellulose membranes were prepared as detailed in the Appendix (section Immunoblotting solutions).

3.2.7 Immunoblot assays

Immunological detection assays were performed in the electrotransferred membranes, following Ponceau S staining. Proper membrane hydration was guaranteed with 1x TBS, and possible non-specific binding sites of primary antibodies were blocked by immersing the membranes in a 5% non-fat dry milk in 1x TBS-T blocking solution for 1-2 hours at RT, with gentle agitation. The incubation with the primary antibody was performed according to each manufacturer's instructions, with overnight incubation at 4 ºC followed by 2 hours at RT, and ensuring agitation throughout the whole incubation. After the first incubation, membranes were washed three times for 10 minutes each, with 1x TBS-T. Further membrane incubation was carried out with the appropriated secondary antibody conjugated to horseradish peroxidase (HRP). The secondary antibody is expected to bind specifically to the primary antibody while incubating for 2 hours at RT with agitation. Both the primary and the secondary antibodies solutions were prepared according to dilution presented in Table 1Table 3. After the last incubation, membranes were again washed with 1x TBS-T for 10 minutes, three consecutive times.

Membranes were subsequently subjected to secondary antibody detection by an enhanced chemiluminescence (ECL) detection method. This method is a light emitting non-radioactive method for detection of specific immobilized antigens, and depends on a specific chemiluminescence reagent (Amersham ECL Select Western Blotting Detection Reagent, GE Healthcare Life Sciences). Detection is based on the oxidation of the luminol substrate by the HRP enzyme, generating chemiluminescence at 425 nm. Membranes were incubated with the working mixture of the chemiluminescent detection reagent for 5 minutes at RT. ChemiDoc Imaging System (Bio-Rad) was used for image acquisition by detection of chemiluminescence. Since the emitted light is directly proportional to the amount of protein, a density analysis of the detected protein bands was performed (ImageLab Software, Bio-Rad). Following detection, the membranes were washed three times with 1x TBS-T and one time with distilled water, after which the membranes were dried at RT and properly stored.

Table 3 - Antibodies used in immunoblot assays: respective target protein, primary and secondary antibody specific dilutions and expected outcome after detection.

Target Protein	Primary antibody	Secondary antibody	Expected WB band(s)
Type I collagen	Anti- type I collagen polyclonal rabbit antibody [Novus Biologicals] Dilution: 1:2000 in 3% non-fat dry milk/TBS-T	Horseradish Peroxidase conjugated α-rabbit IgG Dilution: 1:5000 in 3% non-fat dry milk/1x TBS-T solution	Collagen type I α1 and α2 chains are expected to appear at 139 and 129 kDa, respectively. Dimeric and trimeric collagen forms are expected at ~270 kDa and ~400 kDa, respectively.
SPARC protein (Osteonectin)	Anti-SPARC protein polyclonal rabbit antibody [Novus Biologicals] Dilution: 1:1000 in 3% non-fat dry milk/TBS-T	Horseradish Peroxidase conjugated α-rabbit IgG Dilution: 1:5000 in 3% non-fat dry milk/1x TBS-T solution	Osteonectin is expected to appear around 35 kDa or 37 kDa.

3.2.8 Immunocytochemistry and confocal microscopy analysis

For some specific timepoints, detailed in Table 1, cells were grown on coverslips placed within the 35 mm cell culture dish. At each timepoint, the culture medium was removed, cells were washed three times with PBS, and fixed with a 4% paraformaldehyde in PBS solution, for 15-20 minutes. Cells were again washed three times with PBS, and a permeabilizing PBS solution with 0.2% Triton X-100 was used for 10 minutes to permeabilize cells and improve antibody penetration, since the target proteins are intracellular. After permeabilization, coverslips were washed three times with a PBS-T solution (1x PBS/0.1%Tween 20) to wash away Triton X, and incubated with 1% BSA in PBS-T for 30 minutes to block unspecific antibody binding to unspecific epitopes. Tween 20 is a mild detergent that diminishes unspecific antibody binding by disrupting attractive forces such as non-specific hydrophobic interactions, to decrease noise. The BSA/PBS-T solution was used to dilute both the primary and secondary antibodies to ensure continuous blocking of unspecific interactions. Coverslips were incubated with anti-type I collagen and anti-osteocalcin antibodies according to Table 4. The incubation with each of the primary antibodies was performed for 2 hours, at RT. Unbound primary antibodies were removed by washing the coverslips for three consecutive times with PBS-T, 10 minutes per wash. The secondary antibodies are conjugated with fluorescent-dye that target the host species of the primary antibody; they were used according to the dilutions specified in Table 4. After incubation for 1 hour, the secondary antibody was removed by three consecutive washes with PBS-T, 10 minutes per wash, and coverslips mounted onto microscope glass slides with a drop of DAPI-containing Vectashield antifading reagent (Vector, Burlingame, CA, USA). Solutions used for fixation, permeabilization, and blocking were prepared as stated in the Appendix section (Immunocytochemistry solutions).

Table 4 - Antibodies used in immunocytochemistry assays: respective target protein, primary, and secondary antibody specific dilutions.

Target Protein	Primary antibody	Secondary antibody
Type I collagen	Anti-type I collagen polyclonal rabbit antibody [Novus Biologicals] Dilution: 1:500 in 1% BSA/PBS-T solution	Alexa594-conjugated α-rabbit IgG Dilution: 1:300 in 1% BSA/PBS-T solution
Osteocalcin	Anti-osteocalcin monoclonal mouse antibody [Novus Biologicals] Dilution: 1:50 in 1% BSA/PBS-T solution	Alexa488-conjugated α-mouse IgG Dilution: 1:300 in 1% BSA/PBS-T solution

Coverslips were sealed with nail polish to prevent drying and movement under the microscope and stored in the dark at 4 ºC until further analysis by fluorescence laser scanning confocal microscopy (LSCM). Image acquisition was performed with a Zeiss LSM 880 with Airyscan confocal microscope (Zeiss, Jena, Germany). The laser line and the excitation and emission wavelengths of the fluorophores used for image acquirement are summarized in Table 5.

Table 5 - Excitation and emission wavelengths of the fluorophores conjugated with the secondary antibodies, LSCM lasers, and channels used to detect them.

Channel and correspondent color	Excitation Wavelength	Emission Wavelength	Laser line
DAPI (blue) channel	401	421	Laser Diode 405nm 30 mW
Alexa488 (green) channel	490	525	Laser Argon multiline (458/488/514nm) 25mW
Alexa594 (red) channel	590	617	Laser DPSS 561nm 20mW

3.2.9 Alizarin Red-based assays for mineralization

Alizarin red S (ARS) is an anthraquinone dye that has been widely used in staining techniques to evaluate calcium deposits in cell culture. The use of this dye in staining techniques is particularly versatile since it can be extracted from the stained monolayer and assayed. Indeed, following a protocol defined by Gregory and Grady Gunn in 2004[112], ARS can be recovered and semi-quantified via colourimetric detection. At defined timepoints (DIV in Table 1), cells were washed with PBS and incubated with a 4% paraformaldehyde PBS solution for 15 minutes at RT. Cells were washed with distilled water and fixed cells where incubated with a 40 mM ARS stock solution (pH 4.1) (Sigma-Aldrich) for 20 minutes at RT with gentle agitation. The unincorporated staining solution was washed away with distilled water by repeating 4 washes for 5 minutes each. Stained cell layers were observed in a Nikon Eclipse Ti-U microscope. After visualization, the cell layer was incubated with acetic acid (10% v/v) for 30 minutes with agitation at RT and harvested with a cell scraper. The collected slurry was subject to a series of steps: vortexing for 30 seconds, heating for 10 minutes at 85 ºC (with previous parafilm sealing), followed by an incubation on ice for 5 minutes and finishing with centrifugation at 20,000 g for 15 minutes. A 500 µL aliquot of the supernatant was neutralized with 200 µL ammonium hydroxide (10% v/v). From each neutralized aliquot, 150 µL triplicates were plated in a 96-well plate (technical replicates), along with ARS standards, and their absorbance was read at 405 nm in a microplate reader (Infinite 200 PRO, Tecan). ARS standards were prepared from a 4 mM stock solution by consecutive dilutions and aliquoted in triplicates of 150 µL per well into a 96-well plate along with the standard dilution solution considered as blank. The ARS standards were prepared and plated as detailed in Table 6.

Table 6 - ARS standards prepared by consecutive (1:2) dilutions of the 4 mM ARS stock solution.

Stock Solution for Standards (mM)	**Standard # (mM)**							
	Std #1	Std #2	Std #3	Std #4	Std #5	Std #6	Std #7	Blank
4	2	1	0.5	0.25	0.125	0.0625	0.0313	-

The ODs of the replicate wells were averaged to obtain a single OD value for each sample, ARS standard, and blank. The corrected OD value for every sample and standard was calculated by subtracting the average OD value of the blank, according to Equation 3:

$$\begin{aligned} Corrected\ OD\ values\ for\ samples\ (405nm) &= OD(405nm)_{[samples]} - D(405nm)_{[blank]} \\ Corrected\ OD\ values\ for\ standards\ (405nm) &= OD(405nm)_{[standards]} - D(405nm)_{[blank]} \end{aligned} \quad (3)$$

A standard curve was obtained by plotting absorbance as a function of ARS concentration. After determining the equation and R^2 of the trend line, the ARS concentration in each sample was calculated. The final values represent the concentration of ARS incorporated by each sample, what allows for a semi-quantification of the matrix mineralization in that specific condition.

3.2.10 Statistical analysis

The raw values obtained in the experiments were compared to control levels at the first timepoint analysed, converted to percentage, and averaged. The standard deviation (SD) was calculated, and data presented as mean ± SD. Statistical significance analyses of data from control versus stimulated cells conditions were conducted by two-tailed student t-test using the GraphPad Prism software (USA). Differences considered statistically significant are indicated in the respective legends.

4 Results

4.1 Cellular growth and metabolism

4.1.1 MC3T3 cells growth curves

Throughout the length of the assay, the resazurin method was carried out at seven specific timepoints to determine proliferation of metabolic active cells of both control (NS) and stimulated (HF ST) cell populations. As detailed in section 3.2.3, resazurin reduction was measured spectrophotometrically at 570 and 600 nm and cellular viability was calculated using Equation 2 from the cited section. Figure 19 graphically illustrates the proliferation of cells over time.

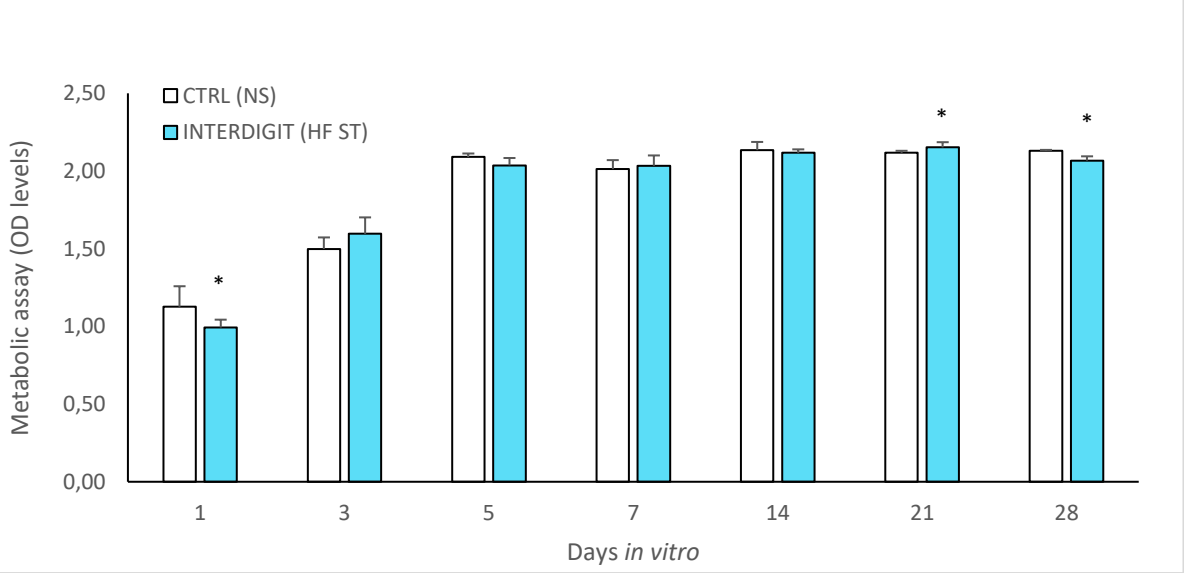

*Figure 19 - Metabolic assay results - OD levels for non-stimulated cells (no stimulus - NS) and high frequency stimulated cells (HF ST) at indicated timepoints. N=3-6 biological replicas. Statistically significant differences, determined by the two-tailed unpaired t-test: *p<0.05, for comparison between HF ST data and NS control values.*

The metabolic activity profile of both cells' populations reveals cellular proliferation until 5 DIV, when it stops and establishes a 'plateau' until 28 DIV. Indeed, from 5 DIV onwards, the metabolic activity maintains values approximately 2 times higher than initial values at 1 DIV. Regarding the electric stimulation, statistical differences were found at 1 and 28 DIV with slightly higher metabolic values for control cells, while at 21 DIV slightly higher metabolic values were found for high frequency stimulated cells.

4.1.2 Temporal profile of protein content

The total protein content in cell lysates was quantified, as described in section 3.2.5, to ensure a normalized loading in SDS-PAGE gels and to provide evidence of the state of protein synthesis throughout the experiment. According to the described procedures, which involve a standard curve equation obtained by plotting BSA absorbance and BSA standard concentration, the total protein concentration was calculated for each biological replica of harvested cell lysates. Figure 20 illustrates total protein content in control (NS) and stimulated cell populations (HF ST) at defined harvesting timepoints.

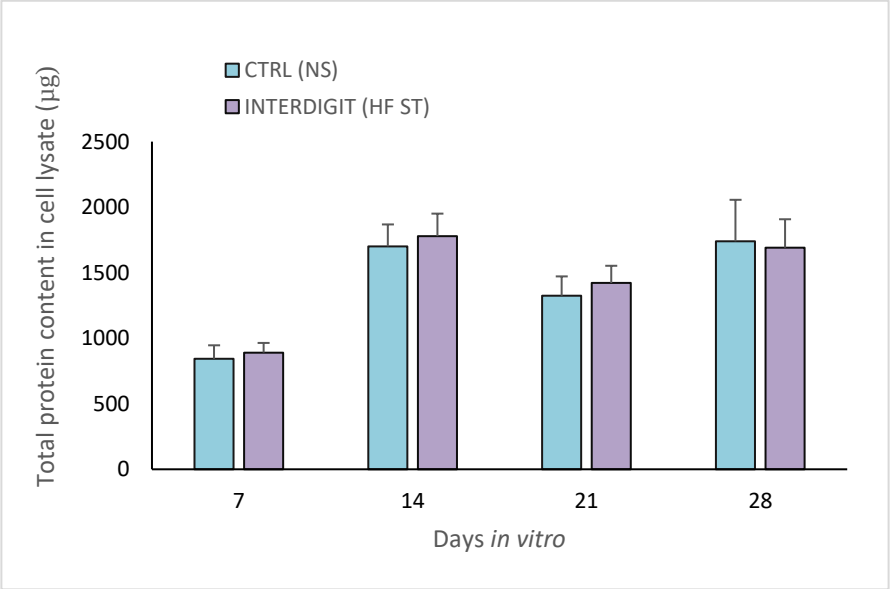

Figure 20 - Total protein content in cell lysates of non-stimulated (NS) and high frequency stimulated (HF ST) cell populations at defined harvesting timepoints. N = 3-5 biological replicas. No statistically significant differences were found between HF ST data and NS control values, as determined by the two-tailed unpaired t-test.

The temporal profile of protein content depicts two periods of higher protein synthesis (14 and 28 DIV) with one intermediate deceleration at 21 DIV. No statistically significant differences were found between both conditions (HF ST and NS), which have shown a similar profile, with identical protein contents regardless of the harvesting timepoint.

4.2 Matrix maturation protein markers

The maturation of the ECM was confirmed by assessing the expression of type I collagen and osteonectin (a non-collagenous protein), and by evaluating the enzymatic activity of ALP. ALP was assessed via a biochemical reaction, while collagen and osteonectin were assessed by immunoblot. Relative quantification of their levels was accomplished through analysis of specific protein bands' densities in chemiluminescent images. Quantification results are expressed as percentage over the control non-stimulated levels at 1 DIV (taken as 100% for collagen and osteonectin secretion) or at 7 DIV (taken as 100% for collagen and osteonectin synthesis). These quantifications are directly comparable between both cell populations (NS and HF ST) since samples were loaded in the same gel and after total protein normalization.

4.2.1 Alkaline phosphatase activity

As described in section 3.2.4, ALP activity was assessed in cell conditioned media (secreted enzyme activity) and in permeabilized harvested cells (intracellular enzyme activity). The absorbance values from biological replicas were averaged and converted into fold increase (FI) percentages over the ALP activity value of control NS cells at 7 DIV (first timepoint of ALP evaluation, taken as 100%). Figure 21 illustrates the profile of secreted ALP activity throughout time, in NS and HF ST cell populations.

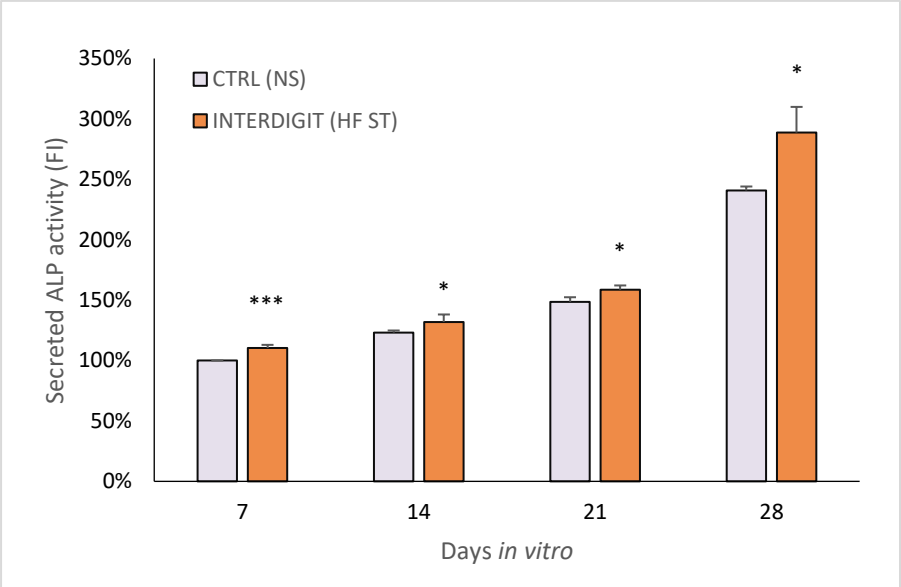

*Figure 21 – Secreted ALP activity throughout time in non-stimulated (NS) and high frequency stimulated (HF ST) cell populations, expressed as fold increase (FI) percentages against ALP activity levels of control samples at 7 DIV. N = 5-10 biological replicas. Statistically significant differences, determined by the two-tailed unpaired t-test: *p<0.05, ***p<0.001, for comparison between HF ST data and NS control values.*

The secreted ALP activity graph shows that cells increase ALP activity throughout time. The secretion pattern for HF ST cells generally resembles the control pattern, but always with slightly and significantly higher levels. At the final 28 DIV timepoint, the ALP activity in media shows the highest values, with HF ST values being approximately 1.2 times higher than control samples' ones.

Figure 22 illustrates the fold increase percentages of intracellular ALP activity throughout time in NS and HF ST cell populations.

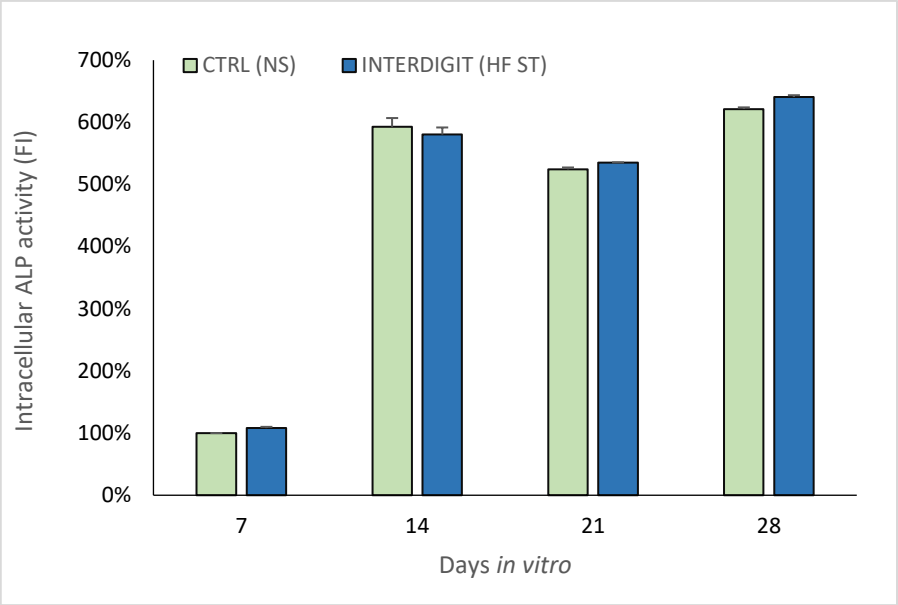

Figure 22 – Intracellular ALP activity throughout time in non-stimulated (NS) and high frequency stimulated (HF ST) cell populations, expressed as fold increase (FI) percentages against ALP activity of control cells at 7 DIV. N = 2 biological replicas.

The intracellular ALP activity pattern follows a profile like the one of total protein in cell lysates (Figure 20), presenting two peaks, one at 14 and one at 28 DIV, with a slight reduction at 21 DIV. The slight differences verified when comparing HF ST with NS cell populations at 7 DIV show apparent increases in intracellular ALP activity for stimulated cells at 7 DIV (1.08 times higher), 21 DIV (5.35 times higher) and 28 DIV (6.41 times higher). At 14 DIV, a minimum decrease in intracellular ALP activity is noted for stimulated cells (0.02 times lower than control for that timepoint).

4.2.2 Expression and secretion of type I collagen

The major component of bone ECM is type I collagen, hence considerable expression levels are expected throughout the entire length of the assay. Collagen was quantified after its immunological detection in WB membranes (detailed in section 3.2.7). An interesting feature of this osteogenic marker is its distinct protein conformations. The antibody used in this work is able to detect monomeric type I collagen chains as well as dimeric forms, trimeric forms and fibres, particularly under denaturing conditions. The secretion profile of type I collagen in conditioned media is illustrated in Figure 23,

alongside with quantifications of the detected collagen bands' densities for each condition and timepoint (Figure 24).

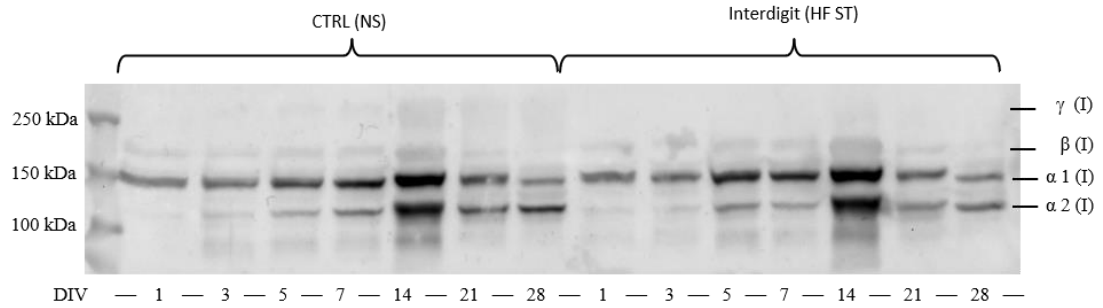

Figure 23 - Immunoblot analysis of type I collagen secretion in conditioned media of non-stimulated (NS) and high frequency stimulated (HF ST) cell populations at defined timepoints (DIV, days in vitro). α 1 (I) and α 2 (I), procollagen monomeric chains; β (I), procollagen dimeric forms and γ (I), procollagen trimeric forms. Migration of molecular weight markers is shown on the left. N=4 biological replicas.

In Figure 23, the immunoblot analysis illustrates type I collagen bands with clear distinction between α 1 (I) and α 2 (I) procollagen monomeric chains and β (I) procollagen dimeric forms. γ (I) procollagen trimeric forms are also distinguishable in slightly less dense bands.

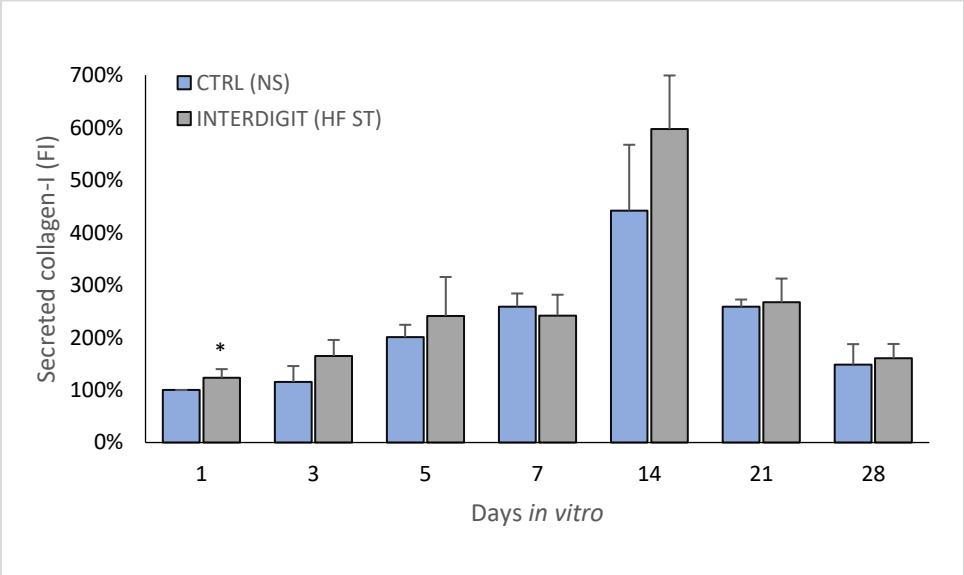

*Figure 24 – Relative quantification of type I collagen in conditioned media throughout time in non-stimulated (NS) and high frequency stimulated (HF ST) cell populations, expressed as fold increase (FI) percentages over collagen secretion values of control cells at 1 DIV. N=4 biological replicas. Statistically significant differences, determined by the two-tailed unpaired t-test: *p<0.05, for comparison between HF ST data and NS control values.*

The general trend demonstrates that type I collagen secretion into conditioned media increases until the 14 DIV timepoint, where the expression is 4.5 to 6 times higher when comparing to the first assessed timepoint (1 DIV). After this peak, expression levels decrease, with the values at 21 DIV being similar to 7 DIV ones, while 28 DIV values diminish to levels similar to the ones of the 3 DIV timepoint. Generally, secretion levels under high frequency stimulation tend to slightly overcome the control levels, but only significantly different at 1 DIV. Also, secretion increase 1.65 times after 3 DIV stimulation; 2.41 times after 5 DIV and approximately 6 times after 14 DIV stimulation – all raises compared to control levels at 1 DIV.

A more complete analysis of type I collagen is possible by assessing its intracellular expression by immunoblot relative quantification. The expression profile of type I collagen in cell lysates is depicted (Figure 25) and quantified for each condition and timepoint analysed (Figure 26).

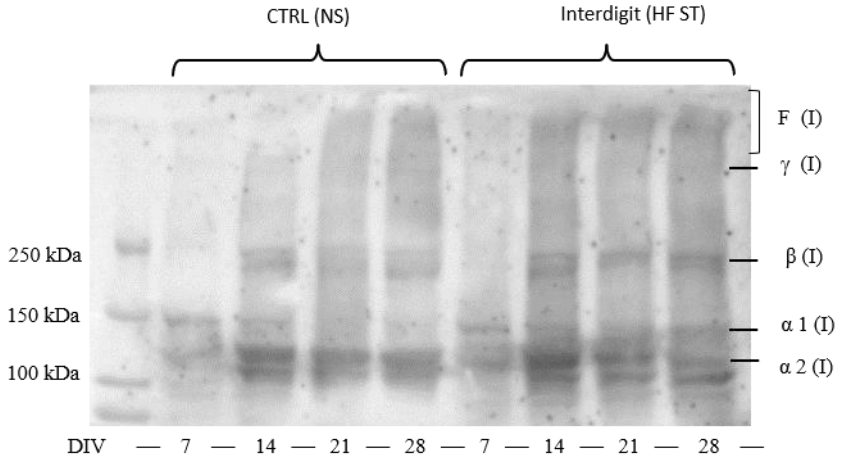

Figure 25 - Immunoblot analysis of type I collagen expression in cell lysates of non-stimulated (NS) and high frequency stimulated (HF ST) cell populations at defined timepoints (DIV, days in vitro). α 1 (I) and α 2 (I), procollagen monomeric chains; β (I), procollagen dimeric forms; γ (I), procollagen trimeric forms and F (I), collagen fibres, type I. Migration of molecular weight markers is shown on the left. N=3 biological replicas.

In Figure 25, the immunoblot analysis illustrates type I collagen bands with clear distinction between α 1 (I), α 2 (I) procollagen monomeric chains, β (I) procollagen dimeric forms and a more diffused γ (I) procollagen trimeric form. Also, cell layer-associated fibrils F (I) are distinguishable in the upper region of the membrane (above 400 kDa).

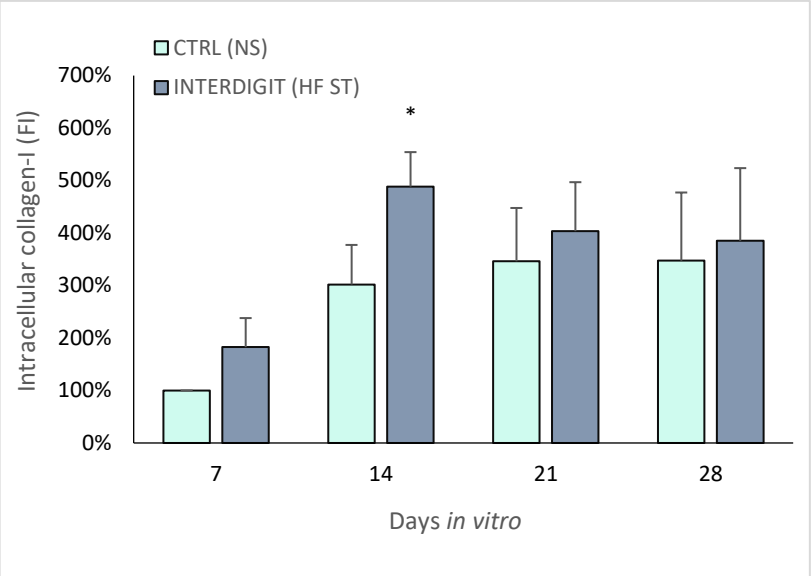

*Figure 26 - Relative quantification of type I collagen (alpha, beta, and gamma forms) in cell lysates throughout time in non-stimulated (NS) and high frequency stimulated (HF ST) cell populations, expressed as fold increase (FI) percentages against relative expression values of control at 7 DIV. N = 3 biological replicas. Statistically significant differences, determined by the two-tailed unpaired t-test: *p<0.05, for comparison between HF ST data and NS control values.*

In control cells, type I collagen expression increases from 7 to 21 DIV, the timepoint when it establishes a 'plateau' maximum level. Electric stimulation induces an expression peak earlier, at 14 DIV, from when it slightly decreases, also establishing a 'plateau' at 21 DIV. Type I collagen expression levels tend to be increased by electric stimulation throughout the complete assay, with significant differences at 14 DIV (1.6 times higher for HF ST cells over control levels at the same timepoint).

4.2.3 Expression and secretion of osteonectin

Osteonectin is one frequently assessed NCP, especially active during osteoblast maturation. This glycosylated protein can also be quantified after immunological detection in WB membranes. The expression and secretion profiles in cell lysates and conditioned media are illustrated in Figure 27 and Figure 29, alongside with the quantifications of the protein bands' for each condition and timepoint (Figure 28 and Figure 30).

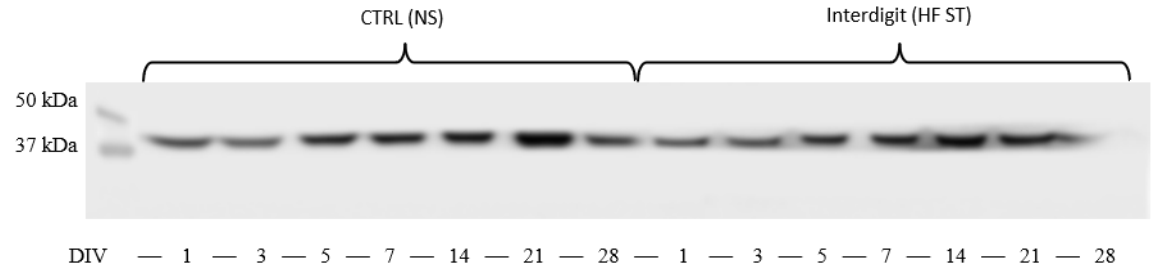

Figure 27 - Immunoblot analysis of osteonectin secretion in conditioned media in non-stimulated (NS) and high frequency stimulated (HF ST) cell populations at defined timepoints (DIV, days in vitro). Migration of molecular weight markers is shown on the left. N=4 biological replicas.

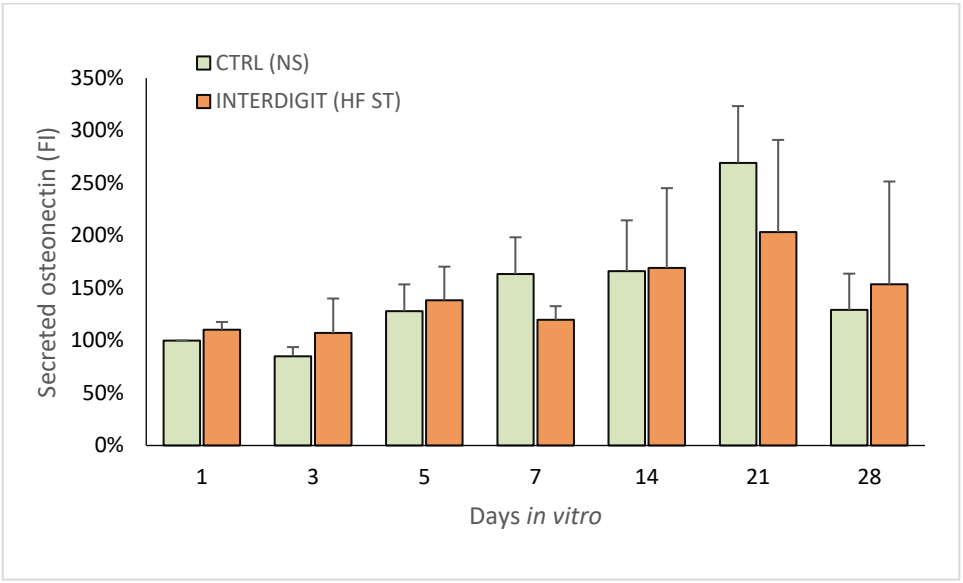

Figure 28 - Relative quantification of osteonectin in conditioned media throughout time in non-stimulated (NS) and high frequency stimulated (HF ST) cell populations, expressed as fold increase (FI) percentages against relative expression values of control cells at 1 DIV. N = 4 biological replicas. No statistically significant differences were found between HF ST data and NS control values, as determined by the two-tailed unpaired t-test.

The general trend demonstrates that osteonectin secretion into the conditioned media is similar for control and high frequency stimulated cell populations, increasing from DIV 1 to 21, when it peaks, and decreasing thereafter. Some oscillations occur, although not statistically different nor constant through time: at 7 and 21 DIV, osteonectin levels in media are slightly decreased for high frequency stimulated cells, and at 3 and 28 DIV osteonectin levels were slightly increased over control levels.

A more complete analysis of osteonectin behaviour throughout differentiation is possible by assessing its intracellular expression. The expression profile in cell lysates is depicted and quantified in the following figures.

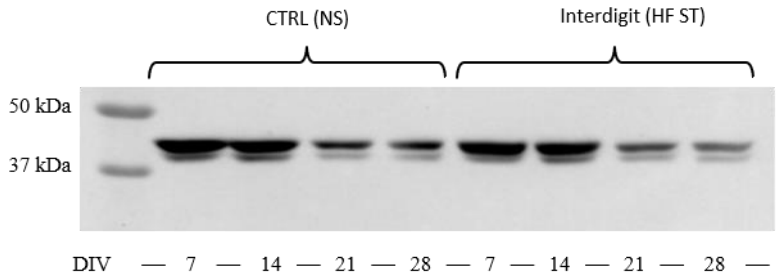

Figure 29 - Immunoblot analysis of osteonectin expression in cell lysates in non-stimulated (NS) and high frequency stimulated (HF ST) cell populations at defined timepoints (DIV, days in vitro). Migration of molecular weight markers is shown on the left. N = 3 biological replicas.

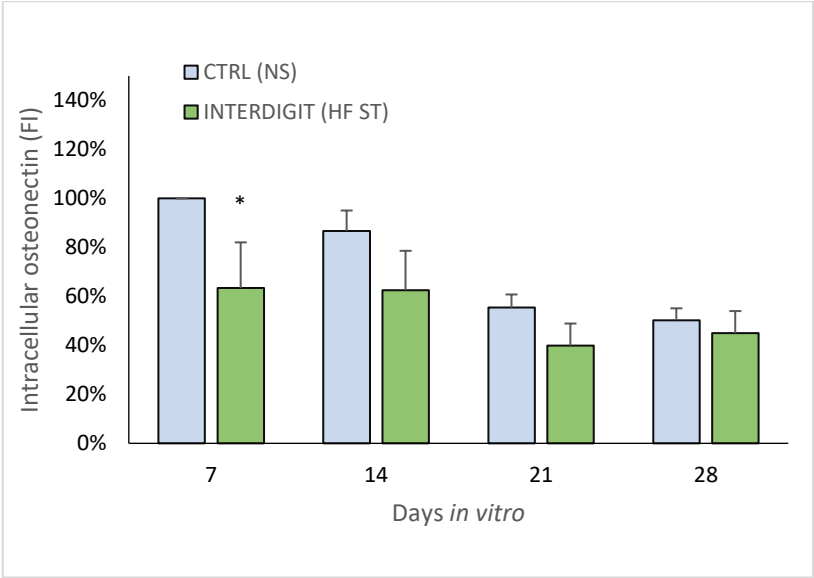

*Figure 30 - Relative quantification of osteonectin in cell lysates throughout time in non-stimulated (NS) and high frequency stimulated (HF ST) cell populations, expressed as fold increase (FI) values against relative expression values of control at 7 DIV. N = 4 biological replicas. Statistically significant differences, determined by the two-tailed unpaired t-test: *p<0.05, for comparison between HF ST data and NS control values.*

The general trend demonstrates that osteonectin intracellular expression is higher at 7 and 14 DIV, and greatly decreases at 21 and 28 DIV, evidences that confirm its role as an early osteogenic marker[103,104]. The profiles are similar between control and high frequency stimulated cell populations, although generally lower for HF ST cells, with a significant decreased expression at 7 DIV for stimulated cells (0.37 times less than control).

4.3 Analysis of matrix mineralization

Mineralization is analysed by quantifying specific markers of osteoblasts' differentiation, like osteocalcin, that according to literature occurs mainly in final stages[10,29]. Also, assessment of mineral levels provides evidence for the mineralization extent in osteoblasts' cultures.

4.3.1 Osteocalcin in the ECM

Immunocytochemistry assays based on primary antibodies against type I collagen and osteocalcin, detected by fluorescent-dye conjugated secondary antibodies, allowed to monitor the localization of these two proteins by immunofluorescence (procedure described in section 3.2.8). Collagen (in red) is visible inside cells, and collagen at the ECM has a diffuse distribution (fibres most likely have a tridimensional conformation not well detected by the antibody). Osteocalcin (in green) is considerably detected throughout the complete cell layer, with higher intensity in stimulated cell populations, where it can be seen intracellularly and particularly abundant in deposits at the ECM.

Figure 31 illustrates control cell populations at 28 DIV, with few osteocalcin accumulation deposits and diffused collagen deposits; co-localization of osteocalcin and collagen occurs only in isolated points. Figure 32 illustrates a comparative image of stimulated cell populations at 28 DIV, with increased number of osteocalcin accumulation deposits and moderately increased number of collagen deposits. Co-localization of osteocalcin and collagen is more frequent under the stimulatory condition.

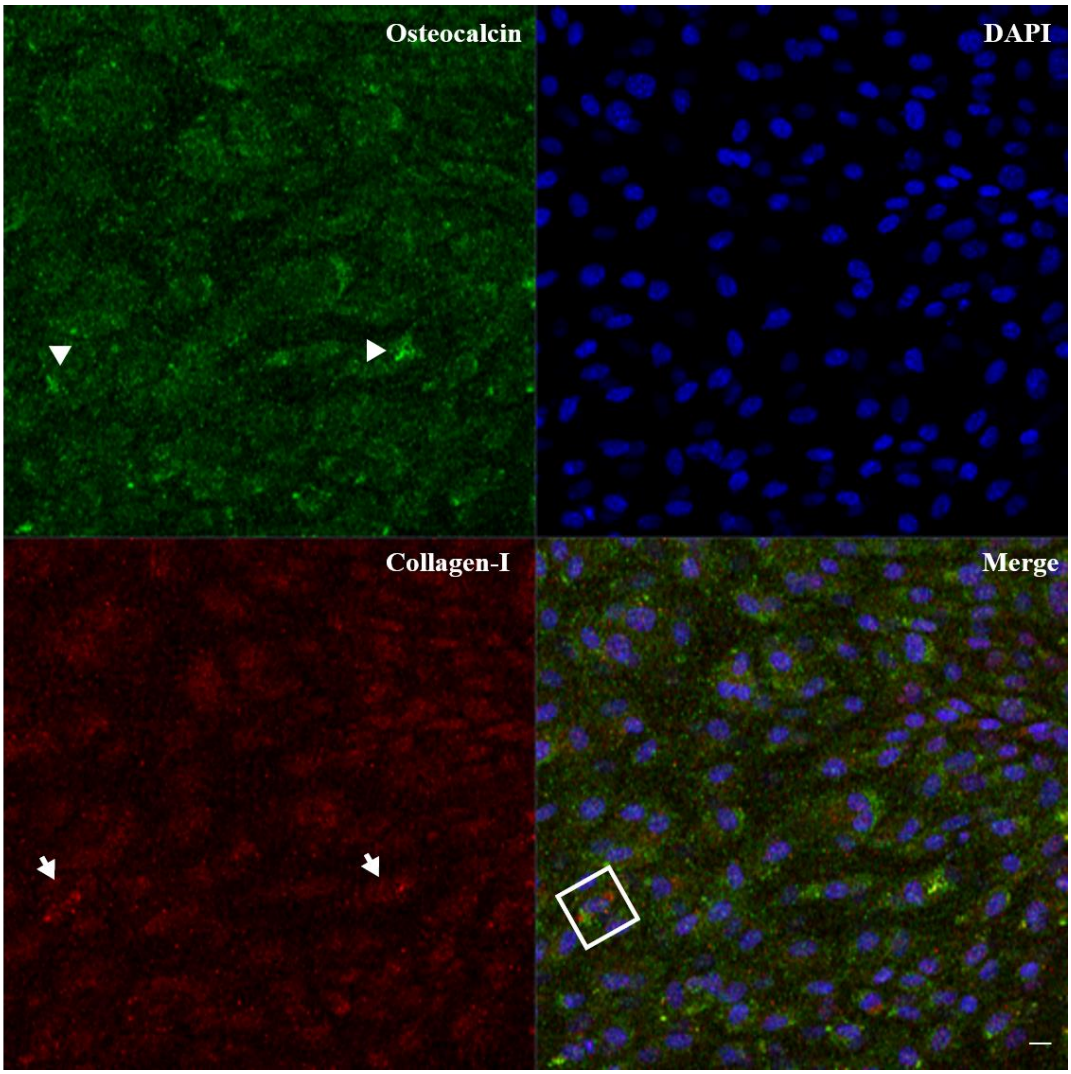

Figure 31 - Confocal microscopy microphotographs of cellular collagen I (in red) and osteocalcin (in green) in control cell populations at 28 DIV. Nuclei is marked with DAPI (in blue). Bar, 20 μm. Arrowheads (▶) indicate osteocalcin accumulation spots. Arrows (➔) indicate collagen accumulation spots. Square in merged image indicates co-localization of osteocalcin and collagen accumulations.

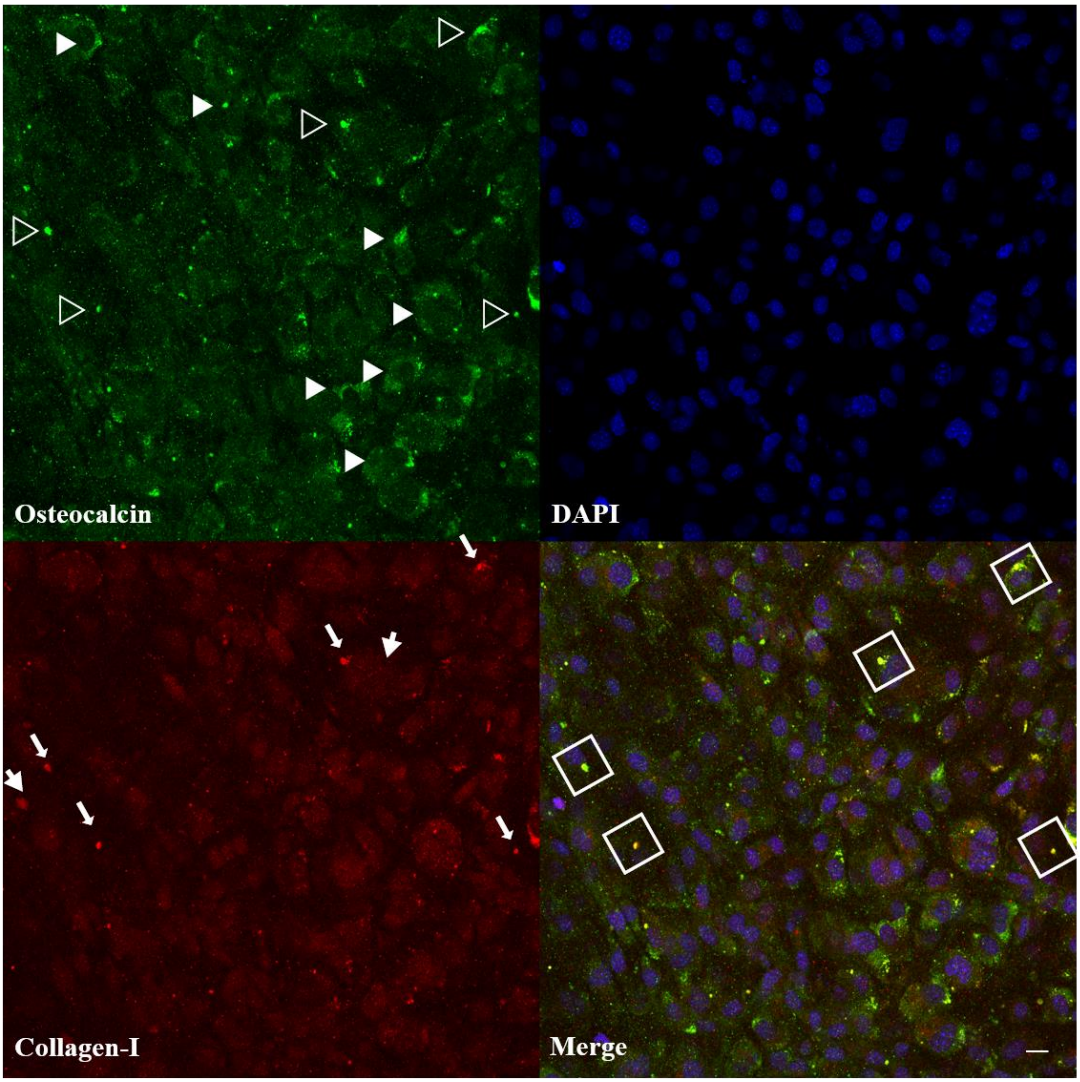

Figure 32 - Confocal microscopy microphotographs of cellular collagen I (in red) and osteocalcin (in green) in high frequency stimulated cell populations at 28 DIV. Nuclei is marked with DAPI (in blue). Bar, 20 μm. Arrowheads (▶) indicate osteocalcin accumulation spots. Arrows (➔) indicate collagen accumulation spots. Arrowheads contour (▷) indicate osteocalcin accumulation spots with co-localization with collagen. Long arrows (➞) indicate collagen accumulation spots with co-localization with osteocalcin. Squares in merged image indicates co-localization of osteocalcin and collagen accumulations.

4.3.2 Calcium deposits (Alizarin Red S assay)

Additional evidence of matrix mineralization may be given by assessment of calcium-rich deposits in the matrix surrounding bone cells, through the quantification of Alizarin Red S (ARS) incorporation (procedure described in section 3.2.9).

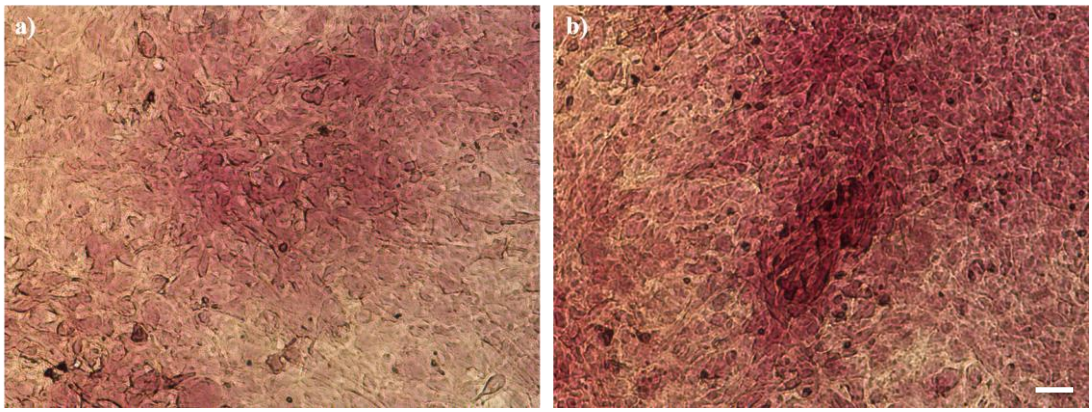

Figure 33 - Alizarin Red S staining of mineralized matrix in osteoblast cells populations at 28 DIV, visualized under a transmitted light microscope. a) non-stimulated cells; b) high frequency stimulated cells. Bar, *50 μm.*

From the light microscopy images (Figure 33), an increased concentration of Alizarin Red dye is noted to be incorporated by the matrix of the osteoblast cultures from the stimulated cell population. The following graph in Figure 34 depicts the quantification (in mM) of incorporated ARS dye in each sample, at the 21 and 28 DIV timepoints.

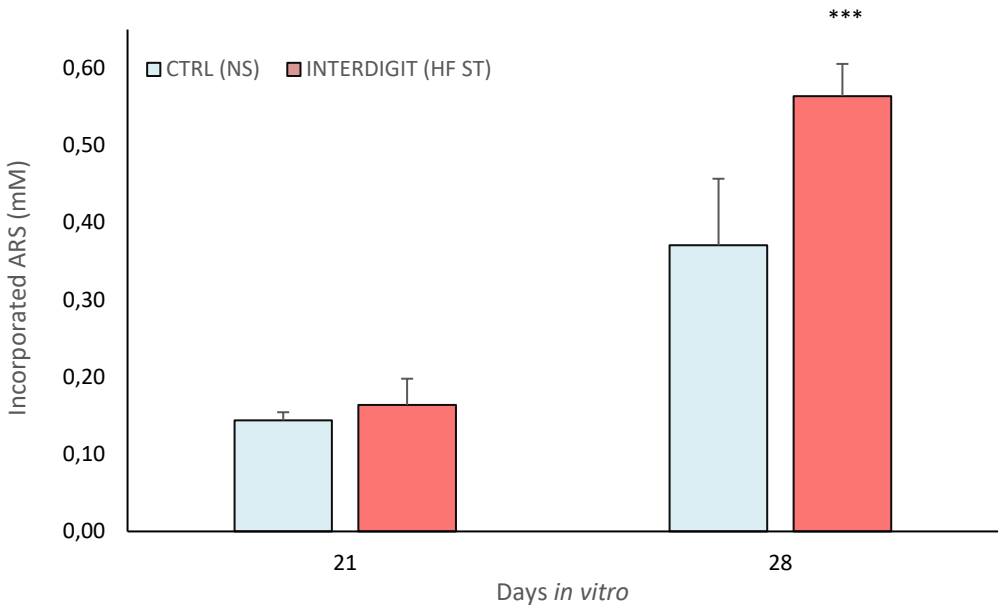

*Figure 34 - Incorporated Alizarin Red S (ARS) stain in non-stimulated (NS) and high frequency stimulated (HF ST) cell populations at 21 and 28 DIV. N = 4-5 biological replicas. Statistically significant differences, determined by the two-tailed unpaired t-test: ***p<0.001, for comparison between HS data and NS control values.*

As expected, the amount of ARS incorporated in the ECM highly increases from 21 to 28 DIV, a timepoint of high matrix mineralization[113]. Further, stimulated cell populations show significantly increased dye incorporation when compared to control cells (NS) at the final timepoint (1.5 times higher).

5 Discussion

Bone fractures, either by accidental causes or due to bone quality impairment (e.g. osteoporosis), represent challenging scenarios both for clinicians and patients. Fracture management and the clinical challenge increase when non-unions or delayed unions occur, leading to surgical procedures (primary or revision) and prolonged hospitalization[114]. This brings personal costs for the patient and societal costs for health care systems. Other musculoskeletal disorders (e.g. osteoarthritis) can result in joint replacement, which is among the most prevalent surgeries performed worldwide and their significant increase is predicted in the forthcoming decades (mainly for young patients)[82]. Facing these scenarios, techniques that improve fracture management and enhance bone union through personalized and non-invasive therapeutics are desirable.

The final goal of the multidisciplinary project that includes the work here described was to analyse the ability of capacitive patterns incorporated into implantable medical devices to deliver osteoconductive electric field stimuli using both low and high frequencies. This was achieved by comparing the complete set of results for both frequencies (14 Hz and 60 kHz) and both stimulator patterns (striped and interdigitated).

Every individual biological experiment was conducted by the same research group from the Institute for Biomedicine (iBiMED) at Universidade de Aveiro. This common denominator ensured that experimental conditions, as well as reagents and equipment, remained unaltered, regardless of the stimulation parameter under testing – allowing for direct comparison between results of different stimulation parameters.

5.1 Cellular proliferation and metabolism

Considering the first stage of osteoblast differentiation *in vitro*, Table 7 summarizes the major biological outcomes for each stimulation parameter tested using the striped and interdigitated CC stimulation patterns. The osteoconductive effects of our stimulation apparatus was compared between: (i) our published data[51] regarding low and high frequency stimulation using striped stimulators; (ii) our unpublished results for low frequency stimulation using interdigitated stimulators and (iii) the newly acquired data here presented, using the same interdigitated stimulator but with high frequency stimulation. The following tables presented in this section summarize the biological outcomes of all CC stimuli tested by our group. In these, the observed effects are compared in low and high frequency stimulated cell populations (LF ST or HF ST) against control cell populations (NS).

Table 7 - Summary of effects of tested CC stimuli in osteoblast proliferation. Results are organized according to stimulator design and stimulation frequency. LF ST and HF ST compared against NS. ND – not described.

Striped Stimulator		
	Metabolic profile with time	Protein content
LF ST (14 Hz; 4h/day)	No significant differences.[51]	Apparently increased levels at 14 DIV; Apparently decreased levels at 28 DIV. (unpublished)
HF ST (60 kHz; 30min/day)	10 % increase over control values at 5 DIV; 15 % increase over control values at 14 DIV.[51]	ND
Interdigitated Stimulator		
	Metabolic profile with time	Protein content
LF ST (14 Hz; 4h/day)	No significant differences. (unpublished)	Apparently increased levels at 14 DIV; Apparently decreased levels at 28 DIV. (unpublished)
HF ST (60 kHz; 30min/day)	Significant 14 % decrease over control values at 1 DIV.	No significant differences.

The metabolic resazurin assay, performed throughout the 28 experimental days, allowed to determine a growth curve – Figure 19 – where cellular proliferation of high frequency stimulated cells follows a profile equal to the one of control cells. For both these conditions, proliferation values increase until 5 DIV and stabilize from 7 DIV timepoint onwards, with the MC3T3 osteoblast proliferation period mainly occurring in the first 5 days in vitro. Although similar, statistically significant differences were found at 1 DIV, what reveals that high frequency stimulation using interdigitated electrodes might delay initial cellular proliferation. The statistical differences at 21 DIV and 28 DIV show that metabolic activity undergoes a slight increase at 21 DIV under stimulation and further decreases in the following week, which might reveal that cells are fully mature and prepared for mineralization earlier if stimulated. Our published results[51] for striped electrodes at the same high frequency illustrate that proliferation values in stimulated cells overcome control values at 5 DIV and 14 DIV. Hence, striped electrodes described in the literature perform better at earlier timepoints while interdigitated ones increase metabolic activity in later timepoints, possibly for a successful cellular mineralization that occurs earlier than expected due to HF stimulation effects.

The temporal profile of protein content in cell lysates (Figure 20) depicts a similar trend for both control and stimulated cell populations, and no significative differences were noticed. Metabolic activity analysed by resazurin assay shows relatively stable values for all the 4 timepoints when protein content was quantified (7, 14, 21 and 28 DIV). However, 2 periods of increased protein synthesis occur at 14 DIV and 28 DIV with an uncommon deacceleration at 21 DIV. The values at 21 DIV might look a little unusual, although not alarming since the same trend occurs for both conditions under test. An increased protein secretion might justify the decrease in cellular content, and indeed our WB assays point to a highly secretion period between 14 and 21 DIV. The increased values in the following timepoint at 28 DIV may evidence the cell commitment to mineralization.

Studies on bioenergetics during osteoblast differentiation show that glycolysis rate increases in mature osteoblasts and during mineralization, accounting for ~50% of bone cell energy requirements[115]. Such increases are consistent with considerable amounts of mitochondria presenting high transmembrane potential[115]. These features are common for

osteoblasts differentiation and mineralization, which supports the periods of increased protein synthesis at 14 DIV (the maturation peak) and at 28 DIV (the mineralization peak).

The same studies reveal that glycolysis inhibition rapidly decrease ATP levels, suggesting that the respiratory process cannot compensate for loss of glycolytic activity. This major energy generation by glycolysis ensures advantage when bone O_2 supply varies or if energy demands change[115]. Since the protein content of our HF stimulated cells remains like control levels, high frequency stimulated cells are likely to keep this adaptative advantage.

5.2 Matrix maturation

Considering the intermediate stage of osteoblast differentiation *in vitro* and following the comparison described in the previous section, the major biological outcomes for each stimulation parameter were summarized in the Table 8.

Table 8 - Summary of effects of tested CC stimuli in osteoblast maturation. Results are organized according to stimulator design and stimulation frequency. LF ST and HF ST compared against NS. ND – not described.

Striped Stimulator			
	Type I collagen	ALP	Osteonectin
LF ST (14 Hz; 4h/day)	Significant increase in the intracellular levels at 14 DIV (2.45 times higher than control at 7 DIV).[51]	No significant differences for intracellular ALP activity at 15DIV.[51]	No significant differences for intracellular levels.[51]
HF ST (60 kHz; 30min/day)	Significant increase in the intracellular levels at 14 DIV (2.7 times higher than control at 7 DIV).[51]	No significant differences for intracellular ALP activity at 15DIV.[51]	No significant differences for intracellular levels.[51]
Interdigitated Stimulator			
	Type I collagen	ALP	Osteonectin
LF ST (14 Hz; 4h/day)	Increased intracellular deposition at 28 DIV visualized in microphotographs. (unpublished)	Apparently increased activity of secreted enzyme at 21 and 28 DIV. (unpublished)	ND
HF ST (60 kHz; 30min/day)	Significant increase in the intracellular levels at 14 DIV (~5 times higher than control at 7 DIV).	Significant increased activity of secreted enzyme at 7, 14; enzyme activity doubles from 21 to 28 DIV.	Tendency to decrease expression and secretion; significant intracellular decrease at 7 DIV (0.37 times less than control)

Secreted ALP activity assessed in cell's conditioned media – illustrated in Figure 21 – shows statistically significative increases in enzyme activity for stimulated cell population at every evaluated timepoint. Focusing on the later timepoints, secreted ALP activity doubles from 21 DIV to 28 DIV, allowing to infer an advantageous influence for osteoblast mineralization when high frequency stimulation is applied by interdigitated electrodes. As for our literature results[51], ALP activity values were quantified at 15 DIV in intracellular content and no significant differences were found for either stimulatory frequencies (LF ST and HF ST) with the striped electrode. Our unpublished data for interdigitated electrode using low frequency stimulation show apparently increased ALP activity in media at 21 and 28 DIV. In the present work, using the same electrode architecture with high frequency stimulation, ALP activity in media is considerably increased at all timepoints, even improving the results obtained for the LF ST. Further, intracellular ALP activity is apparently higher for high frequency stimulated cell

population at later timepoint (21 and 28 DIV) and at 7 DIV (close to the starting point of osteoblast maturation), when compared to NS control cells (Figure 22). Thus, electric stimulation used in the present study appears to increase ALP levels and promote enzyme secretion into conditioned media. A complementary analysis by WB targeting ALP protein in both cell lysates and conditioned media would confirm the trend, but the overall high frequency stimulation applied by interdigitated electrodes seems to be the most beneficial condition, increasing both secreted and intracellular ALP activity. Such effects are probably related with increased maturation commitment under stimulation, due to ALP role in earlier timepoints until osteoblastic maturation is complete[103,104]; and with positive effects of electric stimulation on matrix mineralization, due to ALP role in preparing the cell for hydroxyapatite crystal generation and matrix mineralization[18,103,104,116].

Secretion of type I collagen into conditioned media – Figure 23 and Figure 24 – shows a similar behaviour for control and stimulated cell populations, following a general profile that increases until 14 DIV and decreases at 21 DIV and 28 DIV. Such results are supported by the total protein content profile (Figure 20), which increases in cell lysates until 14 DIV – and hence more proteins can be secreted to conditioned medium. At 21 DIV and 28 DIV, collagen secretion into conditioned media is also concordant with literature, since osteoblasts commit to mineralization in later stages and collagen secretion diminishes while mineralization-related proteins like osteocalcin and ALP increase secretion levels[10,18]. Statistical differences in secreted collagen levels were found at 1 DIV, i.e. in the beginning of osteoblast proliferation. Such statistical significance allows to infer that high frequency stimulation with interdigitated electrodes promotes osteoblast differentiation earlier in time, what may explain its slightly but significantly decrease in proliferation at 1 DIV (Figure 19).

Type I collagen expression in cell lysates – Figure 25 and Figure 26 – supports the trend for secreted collagen, due to the peak at 14 DIV and the decreases at 21 and 28 DIV occuring for both expression and secretion. The positive effects of high frequency stimulation over control levels of type I collagen expression occur at all assessed timepoints, but statistically significant differences occur at 14 DIV. Literature results[51] also show significant differences at 14 DIV for both low and high frequencies with striped electrodes, however expression increases only for a maximum of 2.7 times over control at

7 DIV, whereas high frequency under test increases for nearly 5 times over control levels. Noteworthy, the peak in type I collagen secretion and synthesis occurs at 14 DIV, a relevant timepoint with intense protein synthesis (Figure 20).

Osteonectin is another protein associated with the various stages of osteoblast proliferation and differentiation. Overall, secreted osteonectin levels (Figure 28) are similar in both stimulated and control cell populations, however some oscillations occur. Since oscillations are not constant over time and do not present statistical differences, the influence of electrical stimulation on the secretion of this NCP remains unclear. Electric stimulation effects on osteonectin levels during differentiation are clearer when analysing its intracellular expression. Generally, osteonectin synthesis (Figure 30) is reduced by high frequency stimulation with significant effects at 7 DIV (an initial timepoint in osteoblast maturation). The amount of osteonectin available for secretion is significantly reduced – a fact that justifies the apparent decrease of secreted osteonectin at 7 DIV in conditioned media. Although reduced by electric stimulation, intracellular levels remain elevated at 7 and 14 DIV over levels at 21 and 28 DIV, proving that osteonectin is indeed important during osteoblast maturation.

Transition from osteoblast maturation to matrix mineralization requires intermediate coordinated processes involving collagen and accessory proteins. Calcium phosphates are required for stable hydroxyapatite crystals that successfully associate with collagen binding sites. Crystals are, in part, helped to be generated by accessory proteins, such as alkaline phosphatase. ALP actuation appears to increase concentration of inorganic phosphates, used to generate calcium phosphates. Indeed, mineralization in intrafibrillar collagen occurs when pH levels are held at alkaline levels, a fact that correlates with higher ALP activity, since this phosphatase is active at alkaline pH levels[18]. At a chemical level, the crystallization process generates considerable amounts of acid, and acid removal regardless of extracellular acid-base environment ensures that hydroxyapatite precipitation is completed. Acid removal is performed by chloride/proton exchangers (ClC) – responsible for acid uptake at osteoblast membrane facing non-mineralized matrix – and by sodium/hydrogen exchangers (NHE) – responsible for acid elimination after release into extracellular fluid[116]. The observed higher ALP activity and higher collagen in high

frequency stimulated cells suggest that the stimulated cell culture would present a higher amount of matrix mineralization.

5.3 Matrix mineralization

Considering the final stage of osteoblast differentiation *in vitro* and following the comparison described in previous sections, the major biological outcomes for each stimulation parameter were summarized in the Table 9.

Table 9 - Summary of effects of tested CC stimuli in osteoblast mineralization. Results are organized according to stimulator design and stimulation frequency. LF ST and HF ST compared against NS. ND – not described.

Striped Stimulator		
	Type I collagen (visualization in microphotographs)	Alizarin Red
LF ST (14 Hz; 4h/day)	Apparently increased intracellular and extracellular deposition at 21 DIV[51]; apparently increased extracellular deposition at 28 DIV. (unpublished)	Apparently unaltered mineralization over control microphotographs.[51]
HF ST (60 kHz; 30min/day)	Apparently increased intracellular and extracellular deposition at 21 DIV[51].	Apparently reduced mineralization over control microphotographs.[51]
Interdigitated Stimulator		
	Type I collagen (visualization in microphotographs)	Alizarin Red
LF ST (14 Hz; 4h/day)	Increased intracellular deposition at 28 DIV. (unpublished)	Apparently unaltered mineralization over control microphotographs. (unpublished)
HF ST (60 kHz; 30min/day)	Apparently increased deposition from 14 to 28 DIV.	Statistically significant increase (1.5 times) at 28 DIV.

Osteocalcin visualization using confocal microscopy analysis, highlights osteocalcin accumulation in intra and extracellular 'spots' particularly abundant in stimulated cell populations (Figure 32). Such localization pattern occurs according to literature, which reports osteocalcin as a late marker up-regulated in post-proliferative

osteoblasts[10]. Type I collagen pattern under immunocytochemistry assays is not the best using this antibody, since tridimensional conformation is not properly visualized. However, the positive effects of electric stimulation in collagen expression are still noted by accumulation of red collagen 'spots'. Comparing Figure 31 to Figure 32, the increased frequency of osteocalcin and collagen deposits with stimulation is visualized. Moreover, co-localization of both markers occurs in greater extent under electric stimuli. Regarding the possible mechanisms involved, collagen deposition was correlated with the levels of latent Transforming growth factor β1 (TGF- β1) by Lohmann et al.[117]. TGF-β is an important growth factor involved in tissue remodelling and wound healing, thus regulating cell matrix deposition. Specifically, levels of TGF-β1 mRNA and activity were observed by other authors to be significantly increased upon stimulation[7]. Since this signalling molecule mediates osteoblast differentiation effects rather than proliferative ones, the increased collagen deposits visualized in stimulated cell populations may indeed be correlated with increased TGF-β1 levels, and a future evaluation of its levels would complement the work here presented.

ARS staining of calcium-rich deposits provide additional evidence on matrix mineralization. Using this dye, only a semi-quantification of sample mineralization is possible, since the exact concentration of calcium deposits within the matrix cannot be inferred by this method[112]. Still, the method provides highlightable results – with increased values of incorporated ARS (Figure 34) at the end of 28 days under high frequency stimulation (1.5 times higher than control levels for the same timepoint). Light microscope images support quantifications of incorporated dye, since increased staining is clearly visible for stimulated cell population in Figure 33.

This considerably significant increase is in agreement with the ALP activity results that increased until 28 DIV to prepare MC3T3 cells for matrix mineralization. Alizarin Red incorporation in cell populations under stimulus demonstrate that calcium rich deposits considerably occur due to 60 kHz stimulus. Such feature is also concordant with osteocalcin up-regulation and activation, as the protein usually experiments post-translational modifications that originate residues for enhanced calcium binding. It would be interesting to measure intracellular calcium levels, in order to confirm this hypothesis. Moreover, calcium levels stand out as a key cellular event involved in the transduction of

electric stimuli. Considering calcium as a second messenger, significant EFs may cause membrane depolarization in osteoblasts and activation of voltage-gated Ca^{2+} channels (VGCCs), inducing rapid Ca^{2+} influxes[118,119]. Calcium levels also induce effects on cells' differentiation by concomitant changes in Ca^{2+} dynamics and by activation of MAP kinases. Such changes are suggested to influence osteogenesis and matrix formation[120].

CC electric stimulation may also activate a signal transduction pathway started by calcium ion translocation through VGCC channels. Increased Ca^{2+} levels in cell membrane lead to an increase in phospholipase A, that increases prostaglandin E synthesis[121,122]. Prostaglandin E 2 (PGE2) administration stimulates bone formation, however, is not accepted as therapeutic option for skeletal disorders due to side effects. PGE2 pharmacological activities are mediated by four G protein-coupled receptors (GPCRs) and two of them – EP2 and EP4 receptors – are present in bone cells and marrow stromal cells. Some studies suggest EP2 and EP4 agonist as therapeutic options for positive outcomes in bone cells. Indeed, agonists of these receptors enhance bone formation and improve bone healing, namely augmented bone mass and strength via EP4 agonists, and enhanced fracture healing via EP2 agonists[123]. These findings support the beneficial effects of the performed electric stimulation, since EP2 and EP4 receptors may also mediate the referred processes by interaction with increased PGE2 levels after CC stimulation.

6 Concluding remarks

Considering the aims defined for this dissertation, experimental tests based on novel 0.1 mm thick interdigitated electrodes were successfully conducted using MC3T3-E1 cell cultures, and biological outcomes were assessed in each stage of osteoblast differentiation. As expected, positive outcomes for high frequency stimulation using the referred stimulators were verified and the most significant effects occur during later stages. The osteoblast proliferation phase evidenced that high frequency electric stimulation does not inhibit cell proliferation, and generally improves osteoblast maturation and significantly promotes matrix mineralization. Maturation reveals increased type I collagen synthesis and enhanced ALP activity, while matrix mineralization is enhanced due to significant presence of calcium-rich deposits and increased collagen and osteocalcin deposition.

The obtained results were already compared with biological outcomes for the previous tested parameters for some timepoints, but a broad temporal assessment could also be performed allowing for point-to-point comparison over 28 days. A solid temporal comprehensiveness would determine the most beneficial parameters for initial, intermediate and later stages of osteoblast differentiation achieving a combined actuation system in terms of electric stimuli parameters to be sequentially applied.

Innovative therapeutic solutions should account for biological response of surrounding tissues; hence, further testing with bone tissues and even in *in vivo* animal models using a prototype of the future active implant would permit to be closer to a translation of this therapeutic actuation system to the clinics. Moreover, stimulation of bone models simulating osteoporosis would assess biological effects in quality-impaired osteoporotic bone. Overall, in the field of personalized therapeutics, the proposed cosurface prototype will be highly advantageous since it not only allows to be miniaturized, it is stretchable and permits flexible integration inside an implant system, and

can also deliver osteoconductive stimuli. Personalized medicine is comprised in the proposed stimulatory system by assessment of osteointegration states (component under development), and by enabling application of time-dependent stimulation of therapeutic stimuli accordingly. The final and ideal therapeutic outcome is the avoidance of revision procedures, since an everlasting operation throughout the patients' lifetime is ensured.

7 References

1. Drake, R. L., Vogl, W. & Mitchell, A. W. M. *Gray's Anatomy for Students*. (Churchill Livingstone, 2014).
2. David W. Dempster. Chapter 2. Anatomy and Functions of the Adult Skeleton. in *Primer on the Metabolic Bone Diseases and Disorders of Mineral Metabolism* (American Society for Bone and Mineral Research, 2006).
3. Arnett, T. Regulation of bone cell function by acid-base balance. *Proc. Nutr. Soc.* **62**, 511–520 (2003).
4. Taichman, R. S. Blood and bone: two tissues whose fates are intertwined to create the hematopoietic stem-cell niche. *Blood* **105**, 2631–2639 (2005).
5. Henry Gray. II. Osteology. in *Anatomy of the Human Body.* (1918).
6. Dorland, S. *Dorland's Pocket 27th Edition Medical Dictionary*. (B. Jain Publishers, 2006).
7. Berk, A. *et al. Molecular Cell Biology*. (Macmillan Learning, 2016).
8. Martini, F. H., Tallitsch, R. B. & Nath, J. L. *Human Anatomy*. (Pearson Education, 2017).
9. Gilbert, S. F. Osteogenesis: The Development of Bones. in *Developmental Biology* (Sinauer Associates, 2000).
10. Jane E. Aubin, Jane B. Lian & Gary S. Stein. Chapter 4. Bone Formation: Maturation and Functional Activities of Osteoblast Lineage Cells. in *Primer on the Metabolic Bone Diseases and Disorders of Mineral Metabolism* (American Society for Bone and Mineral Research, 2006).
11. Jiang, Y. *et al.* Pluripotency of mesenchymal stem cells derived from adult marrow. *Nature* **418**, 41–49 (2002).
12. D Lamplot, J. *et al.* The Current and Future Therapies for Human Osteosarcoma. *Curr. Cancer Ther. Rev.* **9**, 55–77 (2013).
13. Huss, R., Lange, C., Weissinger, E. M., Kolb, H. J. & Thalmeier, K. Evidence of peripheral blood-derived, plastic-adherent CD34(-/low) hematopoietic stem cell clones with mesenchymal stem cell characteristics. *Stem Cells Dayt. Ohio* **18**, 252–260 (2000).
14. Erices, A., Conget, P. & Minguell, J. J. Mesenchymal progenitor cells in human umbilical cord blood. *Br. J. Haematol.* **109**, 235–242 (2000).

15. Church, V. L. & Francis-West, P. Wnt signalling during limb development. *Int. J. Dev. Biol.* **46**, 927–936 (2002).

16. Logan, C. Y. & Nusse, R. The Wnt signaling pathway in development and disease. *Annu. Rev. Cell Dev. Biol.* **20**, 781–810 (2004).

17. ten Dijke, P., Fu, J., Schaap, P. & Roelen, B. A. J. Signal transduction of bone morphogenetic proteins in osteoblast differentiation. *J. Bone Joint Surg. Am.* **85**-A Suppl **3**, 34–38 (2003).

18. Blair, H. C. *et al.* Osteoblast Differentiation and Bone Matrix Formation *In Vivo* and *In Vitro*. *Tissue Eng. Part B Rev.* **23**, 268–280 (2017).

19. Beck, G. R., Zerler, B. & Moran, E. Phosphate is a specific signal for induction of osteopontin gene expression. *Proc. Natl. Acad. Sci.* **97**, 8352–8357 (2000).

20. Hartsock, A. & Nelson, W. J. Adherens and Tight Junctions: Structure, Function and Connections to the Actin Cytoskeleton. *Biochim. Biophys. Acta* **1778**, 660–669 (2008).

21. Meng, W. & Takeichi, M. Adherens Junction: Molecular Architecture and Regulation. *Cold Spring Harb. Perspect. Biol.* **1**, (2009).

22. Lin, G. L. & Hankenson, K. D. Integration of BMP, Wnt, and Notch signaling pathways in osteoblast differentiation. *J. Cell. Biochem.* **112**, 3491–3501 (2011).

23. Biomedical Tissue Research, University of York. Bone remodelling. Osteocord-Bone from Blood.

24. Pamela Gehron Robey & Adele L. Boskey. Chapter 3. Extracellular Matrix and Biomineralization of Bone. in *Primer on the Metabolic Bone Diseases and Disorders of Mineral Metabolism* (American Society for Bone and Mineral Research, 2006).

25. Brodsky, B. & Persikov, A. V. Molecular Structure of the Collagen Triple Helix. in *Advances in Protein Chemistry* **70**, 301–339 (Elsevier, 2005).

26. Gokhale, J., Boskey, A. & Robey, P. The Biochemistry of Bone. in *Osteoporosis* **1**, 107–188 (Elsevier, 2001).

27. Brekken, R. A. & Sage, E. H. SPARC, a matricellular protein: at the crossroads of cell-matrix communication. *Matrix Biol. J. Int. Soc. Matrix Biol.* **19**, 816–827 (2001).

28. Robey, P. G. Bone Matrix Proteoglycans and Glycoproteins. in *Principles of Bone Biology* 225–237 (Elsevier, 2002). doi:10.1016/B978-012098652-1.50116-5

29. Seibel, M. J. Biochemical markers of bone remodeling. *Endocrinol. Metab. Clin. North Am.* **32**, 83–113, vi–vii (2003).

30. Glimcher, M. J. The Nature of the Mineral Phase in Bone: Biological and Clinical Implications. in *Metabolic Bone Disease and Clinically Related Disorders* 23-52e (Elsevier, 1998). doi:10.1016/B978-012068700-8/50003-7

31. Anderson, H. C. Matrix vesicles and calcification. *Curr. Rheumatol. Rep.* **5**, 222–226 (2003).

32. Mescher, A. L. Bone. in *Junqueira's Basic Histology* (McGraw-Hill Education, 2016).

33. Raisz, L. G., Bilezikian, J. P. & Martin, T. J. *Principles of Bone Biology (3rd ed.)*. (Academic Press, 2008).

34. DW Dempster. Bone remodeling. in *Disorders of Bone Miner Metabolism* (eds. FL Coe & MJ Favus) 315–343 (Lippincott Williams and Wilkins, 2002).

35. AM Parfitt. The physiologic and pathogenetic significance of bone histomorphometric data. in *Disorders of Bone Miner Metabolism* (eds. FL Coe & MJ Favus) 469–485 (Lippincott Williams and Wilkins, 2002).

36. Dole, N. Genetic Determinants of Skeletal Diseases: Role of microRNAs. (2015).

37. Roodman, G. D. Cell biology of the osteoclast. *Exp. Hematol.* **27**, 1229–1241 (1999).

38. Burr, D. B. Targeted and nontargeted remodeling. *Bone* **30**, 2–4 (2002).

39. Parfitt, A. M. Targeted and nontargeted bone remodeling: relationship to basic multicellular unit origination and progression. *Bone* **30**, 5–7 (2002).

40. Reddy, S. V. Regulatory mechanisms operative in osteoclasts. *Crit. Rev. Eukaryot. Gene Expr.* **14**, 255–270 (2004).

41. Smit, T. H. & Burger, E. H. Is BMU-coupling a strain-regulated phenomenon? A finite element analysis. *J. Bone Miner. Res. Off. J. Am. Soc. Bone Miner. Res.* **15**, 301–307 (2000).

42. Huiskes, R., Ruimerman, R., van Lenthe, G. H. & Janssen, J. D. Effects of mechanical forces on maintenance and adaptation of form in trabecular bone. *Nature* **405**, 704–706 (2000).

43. Burger, E. H., Klein-Nulend, J. & Smit, T. H. Strain-derived canalicular fluid flow regulates osteoclast activity in a remodelling osteon--a proposal. *J. Biomech.* **36**, 1453–1459 (2003).

44. Currey, J. D. *Bones: Structure and Mechanics*. (Princeton University Press, 2002).

45. Louis C. Gerstenfeld & Thomas A. Einhorn. Chapter 7. Fracture Healing: The Biology of Bone Repair and Regeneration. in *Primer on the Metabolic Bone Diseases and Disorders of Mineral Metabolism* (American Society for Bone and Mineral Research, 2006).

46. Ferguson, C., Alpern, E., Miclau, T. & Helms, J. A. Does adult fracture repair recapitulate embryonic skeletal formation? *Mech. Dev.* **87**, 57–66 (1999).

47. Woolf, A. D. Global burden of osteoarthritis and musculoskeletal diseases. *BMC Musculoskelet. Disord.* **16**, S3 (2015).

48. Storheim, K. & Zwart, J.-A. Musculoskeletal disorders and the Global Burden of Disease study. *Ann. Rheum. Dis.* **73**, 949–950 (2014).

49. March, L. *et al.* Burden of disability due to musculoskeletal (MSK) disorders. *Best Pract. Res. Clin. Rheumatol.* **28**, 353–366 (2014).

50. Vos, T. *et al.* Years lived with disability (YLDs) for 1160 sequelae of 289 diseases and injuries 1990-2010: a systematic analysis for the Global Burden of Disease Study 2010. *Lancet Lond. Engl.* **380**, 2163–2196 (2012).

51. Soares dos Santos, M. P. *et al.* New cosurface capacitive stimulators for the development of active osseointegrative implantable devices. *Sci. Rep.* **6**, (2016).

52. Feller, L. *et al.* Osseointegration: biological events in relation to characteristics of the implant surface. *SADJ J. South Afr. Dent. Assoc. Tydskr. Van Suid-Afr. Tandheelkd. Ver.* **69**, 112, 114–117 (2014).

53. Albrektsson, T. & Johansson, C. Osteoinduction, osteoconduction and osseointegration. *Eur. Spine J. Off. Publ. Eur. Spine Soc. Eur. Spinal Deform. Soc. Eur. Sect. Cerv. Spine Res. Soc.* **10 Suppl 2**, S96-101 (2001).

54. Ramirez-Vick, J. E. Biophysical Stimulation for Bone Regeneration. *JSM Biotechnol. Biomed. Eng.* **1**, 1014 (2013).

55. Gelalis, I. D. *et al.* Diagnostic and treatment modalities in nonunions of the femoral shaft: a review. *Injury* **43**, 980–988 (2012).

56. Reis, J. *et al.* A New Piezoelectric Actuator Induces Bone Formation In Vivo: A Preliminary Study. *BioMed Research International* (2012). doi:10.1155/2012/613403

57. Gan, J. C. & Glazer, P. A. Electrical stimulation therapies for spinal fusions: current concepts. *Eur. Spine J.* **15**, 1301–1311 (2006).

58. Rubin, C. T., Judex, S., Qin, Y.-X. & Rubin, J. Chapter 23 - Prevention of Osteoporosis by Physical Signals: Defining a Potential Role for Nondrug Strategies in the Treatment of Musculoskeletal Injury and Disease. in *Osteoporosis (Fourth Edition)* (eds. Marcus, R., Feldman, D., Dempster, D. W., Luckey, M. & Cauley, J. A.) 517–535 (Academic Press, 2013).

59. Chang, K., Chang, W. H.-S., Tsai, M.-T. & Shih, C. Pulsed Electromagnetic Fields Accelerate Apoptotic Rate in Osteoclasts. *Connect. Tissue Res.* **47**, 222–228 (2006).

60. Tu, K. N. *et al.* Osteoporosis: A Review of Treatment Options. *Pharm. Ther.* **43**, 92–104 (2018).

61. Fukada, E. & Yasuda, I. On the Piezoelectric Effect of Bone. *J. Phys. Soc. Jpn.* **12**, 1158–1162 (1957).

62. Gross, D. & Williams, W. S. Streaming potential and the electromechanical response of physiologically-moist bone. *J. Biomech.* **15**, 277–295 (1982).

63. Griffin, M. & Bayat, A. Electrical Stimulation in Bone Healing: Critical Analysis by Evaluating Levels of Evidence. *Eplasty* **11**, (2011).

64. Black, J. *Electrical stimulation: Its role in growth, repair and remodeling of the musculoskeletal system*. (1986).

65. Kooistra, B., Jain, A. & Hanson, B. Electrical stimulation: Nonunions. *Indian J. Orthop.* **43**, 149 (2009).

66. Balint, R., Cassidy, N. J. & Cartmell, S. H. Electrical Stimulation: A Novel Tool for Tissue Engineering. *Tissue Eng. Part B Rev.* **19**, 48–57 (2013).

67. Saha, S. & Williams, P. A. Electric and dielectric properties of wet human cancellous bone as a function of frequency. *Ann. Biomed. Eng.* **17**, 143–158 (1989).

68. Saha, S. & Williams, P. A. Electric and dielectric properties of wet human cortical bone as a function of frequency. *IEEE Trans. Biomed. Eng.* **39**, 1298–1304 (1992).

69. Sierpowska, J. *et al.* Effect of human trabecular bone composition on its electrical properties. *Med. Eng. Phys.* **29**, 845–852 (2007).

70. Cerrolaza, M., Duarte, V. & Garzón-Alvarado, D. Analysis of Bone Remodeling Under Piezoelectricity Effects Using Boundary Elements. *J. Bionic Eng.* **14**, 659–671 (2017).

71. Gabriel, C., Gabriel, S. & Corthout, E. The dielectric properties of biological tissues: I. Literature survey. *Phys. Med. Biol.* **41**, 2231–2249 (1996).

72. Williams, P. A. & Saha, S. The electrical and dielectric properties of human bone tissue and their relationship with density and bone mineral content. *Ann. Biomed. Eng.* **24**, 222–233 (1996).

73. Coelho, P. G. & Jimbo, R. Osseointegration of metallic devices: current trends based on implant hardware design. *Arch. Biochem. Biophys.* **561**, 99–108 (2014).

74. Moucha, C. S., Urban, R. M., Turner, T. M., Jacobs, J. J. & Sumner, D. R. Fixation of implants. *Jt. Replace. Bone Resorption Pathol. Biomater. Clin. Pract.* 13–52 (2006).

75. Sumner, D. R. & Virdi, A. S. Materials in hip surgery: Bioactive coatings for implant fixation. *Surg. Hip* 145–156 (2013).

76. Sumner, D. R. Long-term implant fixation and stress-shielding in total hip replacement. *J. Biomech.* **48**, 797–800 (2015).

77. Soares dos Santos, M. P., Ferreira, J. A. F., Ramos, A. & Simões, J. A. O. Active orthopaedic implants: Towards optimality. *J. Frankl. Inst.* **352**, 813–834 (2015).

78. Soares dos Santos, M. P. *et al.* Instrumented hip joint replacements, femoral replacements and femoral fracture stabilizers. *Expert Rev. Med. Devices* **11**, 617–635 (2014).

79. Goriainov, V., Cook, R., M. Latham, J., G. Dunlop, D. & Oreffo, R. O. C. Bone and metal: An orthopaedic perspective on osseointegration of metals. *Acta Biomater.* **10**, 4043–4057 (2014).

80. Marco Paulo Soares dos Santos. A new concept model for instrumented active orthopaedic implants. (Doctoral Thesis in Mechanical Engineering - Universidade de Aveiro, 2016).

81. Hronik-Tupaj, M. & Kaplan, D. L. A review of the responses of two- and three-dimensional engineered tissues to electric fields. *Tissue Eng. Part B Rev.* **18**, 167–180 (2012).

82. Kurtz, S. M. *et al.* Future young patient demand for primary and revision joint replacement: national projections from 2010 to 2030. *Clin. Orthop.* **467**, 2606–2612 (2009).

83. Pabinger, C. & Geissler, A. Utilization rates of hip arthroplasty in OECD countries. *Osteoarthritis Cartilage* **22**, 734–741 (2014).

84. Gomes, M. da C. M. F. Modelo biofísico para análise da estimulação eletromagnética no osso. (Masther Thesis in Mechanical Engineering - Universidade de Aveiro, 2017).

85. Brighton, C. T., Tadduni, G. T. & Pollack, S. R. Treatment of sciatic denervation disuse osteoporosis in the rat tibia with capacitively coupled electrical stimulation. Dose response and duty cycle. *J. Bone Joint Surg. Am.* **67**, 1022–1028 (1985).

86. Brighton, C. T., Nichols, C. E. & Arangio, G. A. Amelioration of oxygen-induced osteoporosis in the in vitro fetal rat tibia with a capacitively coupled electrical field. *J. Orthop. Res. Off. Publ. Orthop. Res. Soc.* **3**, 311–320 (1985).

87. Rubin, C. T., McLeod, K. J. & Lanyon, L. E. Prevention of osteoporosis by pulsed electromagnetic fields. *J. Bone Joint Surg. Am.* **71**, 411–417 (1989).

88. Victoria, G., Petrisor, B., Drew, B. & Dick, D. Bone stimulation for fracture healing: What's all the fuss? *Indian J. Orthop.* **43**, 117–120 (2009).

89. Haglin, J. M., Jain, S., Eltorai, A. E. M. & Daniels, A. H. Bone Growth Stimulation: A Critical Analysis Review. *JBJS Rev.* **5**, e8 (2017).

90. Dimitriou, R. & Babis, G. C. Biomaterial osseointegration enhancement with biophysical stimulation. *J. Musculoskelet. Neuronal Interact.* **7**, 253–265 (2007).

91. Bonmassar, G. *et al.* Microscopic magnetic stimulation of neural tissue. *Nat. Commun.* **3**, 921 (2012).

92. Lee, S. W., Fallegger, F., Casse, B. D. F. & Fried, S. I. Implantable microcoils for intracortical magnetic stimulation. *Sci. Adv.* **2**, e1600889 (2016).

93. Marks Jr., S. C. & Odgren, P. R. Chapter 1 - Structure and Development of the Skeleton. in *Principles of Bone Biology (Second Edition)* (eds. Bilezikian, J. P., Raisz, L. G. & Rodan, G. A.) 3–15 (Academic Press, 2002). doi:10.1016/B978-012098652-1.50103-7

94. João Pedro de Almeida Coutinho. Estudo comparativo de atuadores capacitivos para implantes ativos. (Masther Thesis in Mechanical Engineering - Universidade de Aveiro, 2017).

95. Fitzsimmons, R. J., Farley, J. R., Adey, W. R. & Baylink, D. J. Frequency dependence of increased cell proliferation, in vitro, in exposures to a low-amplitude, low-frequency electric field: evidence for dependence on increased mitogen activity released into culture medium. *J. Cell. Physiol.* **139**, 586–591 (1989).

96. Fitzsimmons, R. J., Ryaby, J. T., Mohan, S., Magee, F. P. & Baylink, D. J. Combined magnetic fields increase insulin-like growth factor-II in TE-85 human osteosarcoma bone cell cultures. *Endocrinology* **136**, 3100–3106 (1995).

97. McLeod, K. J., Donahue, H. J., Levin, P. E., Fontaine, M. A. & Rubin, C. T. Electric fields modulate bone cell function in a density-dependent manner. *J. Bone Miner. Res. Off. J. Am. Soc. Bone Miner. Res.* **8**, 977–984 (1993).

98. Soares dos Santos, M. P. *et al.* Instrumented hip implants: electric supply systems. *J. Biomech.* **46**, 2561–2571 (2013).

99. Stein, G. S., Lian, J. B., Stein, J. L., Van Wijnen, A. J. & Montecino, M. Transcriptional control of osteoblast growth and differentiation. *Physiol. Rev.* **76**, 593–629 (1996).

100. Diniz, P., Shomura, K., Soejima, K. & Ito, G. Effects of pulsed electromagnetic field (PEMF) stimulation on bone tissue like formation are dependent on the maturation stages of the osteoblasts. *Bioelectromagnetics* **23**, 398–405 (2002).

101. Cowin, S. C. *Bone Mechanics Handbook, Second Edition*. (Taylor & Francis, 2001).

102. Pina, S. *et al.* Biological responses of brushite-forming Zn- and ZnSr- substituted beta-tricalcium phosphate bone cements. *Eur. Cell. Mater.* **20**, 162–177 (2010).

103. Griffin, M., Sebastian, A., Colthurst, J. & Bayat, A. Enhancement of Differentiation and Mineralisation of Osteoblast-like Cells by Degenerate Electrical Waveform in an In Vitro Electrical Stimulation Model Compared to Capacitive Coupling. *PLoS ONE* **8**, e72978 (2013).

104. Chang, W. H.-S., Chen, L.-T., Sun, J.-S. & Lin, F.-H. Effect of pulse-burst electromagnetic field stimulation on osteoblast cell activities. *Bioelectromagnetics* **25**, 457–465 (2004).

105. Hoang, Q. Q., Sicheri, F., Howard, A. J. & Yang, D. S. C. Bone recognition mechanism of porcine osteocalcin from crystal structure. *Nature* **425**, 977–980 (2003).

106. Wiesmann, H., Hartig, M., Stratmann, U., Meyer, U. & Joos, U. Electrical stimulation influences mineral formation of osteoblast-like cells in vitro. *Biochim. Biophys. Acta* **1538**, 28–37 (2001).

107. Czekanska, E. M., Stoddart, M. J., Richards, R. G. & Hayes, J. S. In search of an osteoblast cell model for in vitro research. *Eur. Cell. Mater.* **24**, 1–17 (2012).

108. Vander Molen, M. A., Donahue, H. J., Rubin, C. T. & McLeod, K. J. Osteoblastic networks with deficient coupling: differential effects of magnetic and electric field exposure. *Bone* **27**, 227–231 (2000).

109. Borra, R. C., Lotufo, M. A., Gagioti, S. M., Barros, F. de M. & Andrade, P. M. A simple method to measure cell viability in proliferation and cytotoxicity assays. *Braz. Oral Res.* **23**, 255–262 (2009).

110. Barnes, S. & Spenney, J. G. Stoichiometry of the nadh-oxidoreductase reaction for dehydrogenase determinations. *Clin. Chim. Acta* **107**, 149–154 (1980).

111. Romero-Calvo, I. *et al.* Reversible Ponceau staining as a loading control alternative to actin in Western blots. *Anal. Biochem.* **401**, 318–320 (2010).

112. Gregory, C. A., Gunn, W. G., Peister, A. & Prockop, D. J. An Alizarin red-based assay of mineralization by adherent cells in culture: comparison with cetylpyridinium chloride extraction. *Anal. Biochem.* **329**, 77–84 (2004).

113. Yan, X.-Z. *et al.* Effects of Continuous Passaging on Mineralization of MC3T3-E1 Cells with Improved Osteogenic Culture Protocol. *Tissue Eng. Part C Methods* **20**, 198–204 (2014).

114. Goldstein, C., Sprague, S. & Petrisor, B. A. Electrical Stimulation for Fracture Healing: Current Evidence: *J. Orthop. Trauma* **24**, S62–S65 (2010).

115. Komarova, S. V., Ataullakhanov, F. I. & Globus, R. K. Bioenergetics and mitochondrial transmembrane potential during differentiation of cultured osteoblasts. *Am. J. Physiol.-Cell Physiol.* (2000).

116. Larrouture, Q. C. *et al.* Chloride-hydrogen antiporters ClC-3 and ClC-5 drive osteoblast mineralization and regulate fine-structure bone patterning in vitro. *Physiol. Rep.* **3**, (2015).

117. Lohmann, C. H. *et al.* Pulsed electromagnetic field stimulation of MG63 osteoblast-like cells affects differentiation and local factor production. *J. Orthop. Res. Off. Publ. Orthop. Res. Soc.* **18**, 637–646 (2000).

118. Özkucur, N., Monsees, T. K., Perike, S., Do, H. Q. & Funk, R. H. W. Local Calcium Elevation and Cell Elongation Initiate Guided Motility in Electrically Stimulated Osteoblast-Like Cells. *PLoS ONE* **4**, (2009).

119. Khatib, L., Golan, D. E. & Cho, M. Physiologic electrical stimulation provokes intracellular calcium increase mediated by phospholipase C activation in human osteoblasts. *FASEB J. Off. Publ. Fed. Am. Soc. Exp. Biol.* **18**, 1903–1905 (2004).

120. Sun, S., Liu, Y., Lipsky, S. & Cho, M. Physical manipulation of calcium oscillations facilitates osteodifferentiation of human mesenchymal stem cells. *FASEB J. Off. Publ. Fed. Am. Soc. Exp. Biol.* **21**, 1472–1480 (2007).

121. Brighton, C. T., Wang, W., Seldes, R., Zhang, G. & Pollack, S. R. Signal transduction in electrically stimulated bone cells. *J. Bone Joint Surg. Am.* **83-A**, 1514–1523 (2001).

122. Kuzyk, P. R. & Schemitsch, E. H. The science of electrical stimulation therapy for fracture healing. *Indian J. Orthop.* **43**, 127–131 (2009).

123. Li, M., Thompson, D. D. & Paralkar, V. M. Prostaglandin E2 receptors in bone formation. *Int. Orthop.* **31**, 767–772 (2007).

Appendix

Cell Culture solutions

PBS (1x)

For a final volume of 500 mL, dissolve one pack of BupH Modified Dulbecco's Phosphate Saline Pack (Pierce) in deionised H_2O.

Final composition:

- 8 mM Sodium Phosphate (Na_2HPO_4)

- 2 mM Potassium Phosphate (KH_2PO_4)

- 140 mM Sodium Chloride (NaCl)

- 10 mM Potassium Chloride (KCl)

Sterilize by filtering through a 0.2µm filter and store at 4 ºC.

10% FBS MEM α

Dissolve in deionised H_2O:

- MEM α (Gibco, Invitrogen): 10.17 g

- Sodium Bicarbonate ($NaHCO_3$) (Sigma): 2.2 g

- 1% (v/v) Streptomycin/Penicillin/Amphotericin solution (Gibco, Invitrogen): 10 mL

- 10% (v/v) FBS (Gibco, Invitrogen): 100 mL

Adjust the pH to 7.2/ 7.3 and adjust the volume to 1000 mL with deiomised H_2O.

Freezing Medium (MEM α – 20% FBS – 5%DMSO)

- Growth medium (MEM α): 8.5mL

- FBS: 1mL

- DMSO (cell culture grade) (Panreac AppliChem, Barcelona, Spain): 0.5mL

ALP substrate solution

Prepare stock solutions in dH_2O:

- Solution A (Na_2CO_3): dilute 0.212 g in 10 mL. Store at 4 ºC.

- Solution B ($NaHCO_3$): dilute 0.168 g in 10 mL. Store at 4 º C.

- 4 mM $MgCl_2$: dilute 0.008 g in 10 mL. Store at 4 ºC.

- 0.02 M NaOH: dilute 0.008 g in 10 mL. Store at room temperature.

ALP substrate (p-Nitrophenyl phosphate) should be prepared fresh (20 mL)

1.Weigh 15 mg of ALP substrate directly into a clean tube

2. Prepare sodium bicarbonate buffer: 2.75 mL solution A + 2.25 mL solution B + 15 mL dH_2O

3. Set pH to 10

4. Add 80.2 µL of $MgCl_2$ solution

6. Protect solution from light

SDS-PAGE and WB solutions

LGB (lower gel buffer) (4x)

To 900 mL of deionised H_2O add:

-Tris base ($C_4H_{11}NO_3$): 181.65 g (1,5 M)

- SDS ($NaC_{12}H_{25}SO_4$): 4 g (0,4%)

Mix until the solutes have dissolved. Adjust the pH to 8.9 and adjust the volume to 1L with deionised H_2O. Store at 4 ºC.

UGB (upper gel buffer) (5x)

To 900 mL of deionised H_2O add:

- Tris base ($C_4H_{11}NO_3$): 75.69 g (0.5 M)

Mix until the solute has dissolved. Adjust the pH to 6.8 and adjust the volume to 1 L with deionised H_2O. Store at 4 ºC.

10% APS (ammonium persulfate)

In 10 mL of deionised H_2O dissolve 1 g of APS. Store at 4 ºC. Stable up to 1 week.

Note: prepare fresh before use.

10% SDS (sodium dodecyl sulfate)

In 10 mL of deionised H_2O dissolve 1 g of SDS.

1% SDS (sodium dodecyl sulfate)

In 9 mL of deionised H_2O dissolve 1 mL of 10% SDS solution.

1 M Tris (pH 6.8) solution

To 150 mL of deionised H_2O add:

- Tris base ($C_4H_{11}NO_3$): 30.3 g

Adjust the pH to 6.8 and adjust the final volume to 250 mL.

Loading Gel Buffer (4x)

-1 M Tris solution (pH 6.8) 2.5 mL (250 mM)

- SDS ($NaC_{12}H_{25}SO_4$): 0.8 g (8%)

- Glycerol ($C_3H_8O_3$): 4 mL (40%)

- β-Mercaptoethanol (C_2H_6OS): 2 mL (2%)

- Bromophenol blue ($C_{19}H_{10}Br_4O_5S$): 1 mg (0.01%)

Adjust the volume to 10 mL with deionised H_2O. Store at room temperature. Protect from light.

Resolving (lower) gel solution for gradient gels

	5% acrylamide solution	20% acrylamide solution
H_2O	9.29 mL	3.67 mL
LGB (4x)	3.75 mL	3.75 mL
Acrylamide	1.88 mL	7.5 mL
APS (10%)	75 µL	75 µL
TEMED	7.5 µL	7.5 µL
Total volume	15 mL	15 mL

Mix both solutions in a gradient system to obtain a 1.5 mm thick resolving gel.

Stacking (upper) gel solution

	3.5% acrylamide solution
H_2O	6.92 mL
UGB (5x)	0.88 mL
Acrylamide	2 mL
APS (10%)	100 µL
SDS (10%)	100 µL
TEMED	10 µL
Total volume	10 mL

Dissolve all components to obtain a 1.5 mm thick stacking gel.

Running Buffer (10x)

To 900 mL of deionised H_2O add:

-Tris base ($C_4H_{11}NO_3$): 30.3 g (250 mM)

- Glycine ($C_2H_5NO_2$): 144.2 g (1.92 M)

- SDS ($NaC_{12}H_{25}SO_4$): 10 g (1%)

Dissolve in deionised H_2O, adjust the pH to 8.3 and adjust the volume to 1 L.

Running Buffer (1x)

In 900 mL of deionised H_2O dissolve 100 mL of 10x Running Buffer solution.

Transfer Buffer (10x)

To 900 mL of deionised H_2O add:

-Tris base ($C_4H_{11}NO_3$): 30.3 g (250 mM)

- Glycine ($C_2H_5NO_2$): 144.2 g (1.92 M)

Dissolve in deionised H_2O, adjust the pH to 8.3 and adjust the volume to 1 L.

Transfer Buffer (1x)

Mix 100 mL of 10x Transfer Buffer, 200 mL of methanol and 700 mL of deionised H_2O.

Immunoblotting solutions

TBS (10x)

To 900 mL of deionised H_2O add:

- Tris base ($C_4H_{11}NO_3$): 12.11 g (10 mM)

- Sodium Chloride (NaCl): 87.66 g (150 mM)

Adjust the pH to 8.0 with HCl and adjust the volume to 1L with deionised H_2O.

TBS (1x)

In 900 mL of deionised H_2O dissolve 100 mL of 10x TBS solution.

TBS-T (10x) (TBS+Tween)

- Tris base ($C_4H_{11}NO_3$): 12.11 g (10 mM)

- Sodium Chloride (NaCl): 87.66 g (150 mM)

- Tween 20: 5 mL (0.05%)

Adjust the pH to 8.0 with HCl and adjust the volume to 1L with deionised H_2O.

TBS-T (1x)

In 900 mL of deionised H_2O dissolve 100 mL of 10x TBS-T solution.

Immunocytochemistry solutions

4% Paraformaldehyde

For a final volume of 100 mL, add 4g of paraformaldehyde to 25 mL deionised H_2O.

Dissolve by heating the mixture at 58 ºC while stirring.

Add 1-2 drops of 1 M NaOH to clarify the solution and filter (0.2 µm filter).

Add 50 mL of 2x PBS and adjust the volume to 100 mL with deionised H_2O.

PBS-T (0.1% Tween)

Dissolve 100 µL of Triton X-100 in 100 mL of 1x PBS.

Cut the end of a blue tip before aspirating Tween 20.

Stir for a long time with the tip inside the bottle.

0.2% Triton X-100

Dissolve 200 µL of Triton X-100 in 100 mL of 1x PBS.

Cut the end of a blue tip before aspirating Triton X-100.

Stir for a long time with the tip inside the bottle.